LA-UR-20-22796
Approved for public release; distribution is unlimited.

Title: LANL studies of ESD spark energy discharge through September 2019

Author(s): Tasker, Douglas George
Cartelli, Laura Bolton
Trujillo, Christopher J.
Hardy, Zachary Kenneth
Webb, Matthew David
Brennan, Colin Reide
Mace, Jonathan Lee

Intended for: Dissemination of work to university contacts

Issued: 2020-04-08

LANL studies of ESD spark energy discharge through September 2019

Douglas Tasker, Laura Cartelli, Christopher Trujillo, Zachary Hardy, Matthew Webb, Colin Brennan and Jonathan Mace

September 2019

Contents

ESD study, Sept 2019

Abstract

Two concentric-sphere apparatuses were used to measure the energies deposited by electric sparks through air to calibrated loads. Both sets of spheres had clean, uninsulated metal surfaces. The 127-mm diameter pair of spheres had a gap of 10 mm and a capacitance of 52 pF. The maximum energy stored on these spheres was 12 mJ and the maximum energy delivered to the 50-mΩ load was 11 μJ, with or without inductance. This load energy amounted to 0.09% of the available input energy; the remainder of the input energy was expended in forming the spark.

The second set of spheres was 330 mm in diameter with a gap of 14 mm and a capacitance of 240 pF. The maximum energy stored on these spheres was 71 mJ and the maximum energy delivered to the 50-mΩ load was 150 μJ *without* added inductance. This load energy was 0.27% of the input energy; again, the remainder of the input energy was expended in forming the spark.

The inclusion of 250 nH and 500 nH inductances in the discharge path of the smaller spheres caused the current discharges to resonate, but had little effect on the maximum energies deposited in the loads. At the time of writing, inductances had not yet been added to the larger spheres.

The magnitudes of the observed spark discharges were stochastic, so more than 1200 tests were required to develop the statistical bounds of the spark behavior, i.e., to estimate the worst case (highest likely) energy depositions in the loads.

The action integrals of the current discharges $\int i^2 dt$ were found to be approximately independent of the load resistances for loads of less than ~1 Ω. Hence the energy deposition scaled with resistance as 207 μJ/Ω and 2.93 mJ/Ω for the two apparatuses.

Introduction

The protection of explosives systems from unintended initiation by electrostatic discharge (ESD) is critically important to the DOE complex. Significant resources are expended each year on the protection of ordnance from ESD initiation. The following experiments were designed at the Los Alamos National Laboratory (LANL) to quantify the electrical energy delivered by electrically conductive objects to target loads under well-controlled conditions.

In a typical accident scenario a body, such as a person or piece of equipment, is electrically charged by friction against insulating surfaces like carpets. The voltages generated can be as high as 30 kV, more typically 20 kV, depending on the prevailing atmospheric conditions, (altitude, humidity, temperature). In some manner that charged body is brought close enough to the explosives that the air breaks down between the body and the explosives and a spark or arc is formed. The electrical energy conveyed by the spark to the explosives may cause initiation, depending on the magnitude of the energy deposited in the explosives[*].

The protocols developed to protect the explosives are based on the assumption that 100% of the available electrostatic energy is available to initiate the explosives. However, from this experimental study and various theoretical studies including those at the Colorado School of Mines [1], it is found that a large fraction of the electrostatic energy on the body is dissipated in forming the spark in air; in this study the fraction typically exceeded 99% of the available energy. Consequently, a small fraction of the original electrostatic energy (<1%) is actually delivered to the target load. This paper quantifies that energy fraction for various conditions of ESD and various resistive and inductive loads.

Spark formation

A simplified picture of the spark channel formation is that a current-carrying filament is formed in the gas due to localized ionization in regions of high electric field, followed by corona, and leader formation. Joule heat is deposited in this filament, which causes an increase in the gas pressure and expands the filament. The filament eventually becomes a channel that is hot enough to ionize the gas and form plasma; this will expand at supersonic velocities as a shockwave. The formation of this hot channel expends a significant fraction of the energy; this expended energy is consequently not available to initiate the target load, e.g., explosives*.

This report describes experiments in which concentric metal spheres are charged to known energetic states under controlled conditions and then discharged into target loads. The energy dissipated in the load is recorded and compared to the original energy.

[*] This work is part of a study that considers not only coupling energy directly to explosives, but also coupling to other components such as insulators, detonator cables, electrically sensitive components, etc.

LANL Concentric Spheres Experiment, Bare Metal Surfaces

Description of spheres

In these experiments two concentric-sphere apparatuses were used to study the spark discharges. The first was a 127-mm (5-inch) diameter pair of spheres with a gap of 10 mm and a capacitance of 52 pF. The maximum energy stored on the 5-inch spheres was determined by the maximum voltage difference that could be achieved between the spheres and the capacitance, it was 12 mJ and the maximum energy delivered to the 50-mΩ load was 11 μJ, *with or without* inductance.

The second set of spheres was 330 mm (13-inch) in diameter with a gap of 14 mm and a capacitance of 244 pF, Figure 2. The maximum energy stored on these 13-inch spheres was 71 mJ and the maximum energy delivered to the 50-mΩ load was 150 μJ *without* added inductance. The general features of the apparatuses are shown in Figure 1 for the 5-inch sphere set. The metal surfaces of both spheres were clean, bare aluminum. The inner sphere of the 5-inch apparatus was solid aluminum whereas that of the 13-inch sphere was hollow to reduce mass. The two halves of the 13-inch inner sphere were welded together on the equator.

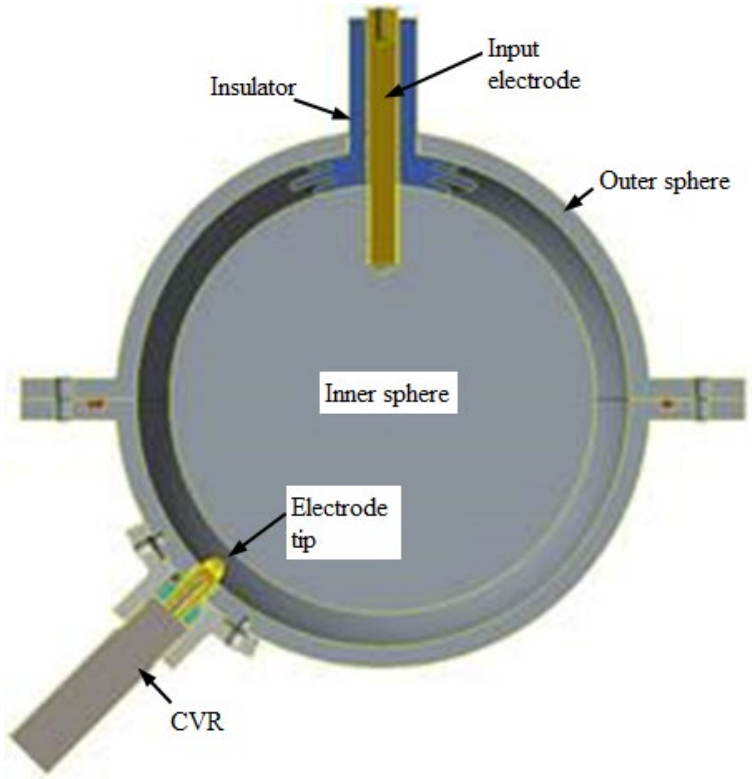

Figure 1. 5-inch apparatus showing the input electrode / suspension rod and insulator at the top, the CVR and electrode tip at the bottom. The spheres are separated by an air gap of 10 mm.

In Figure 1 the center sphere was suspended and charged via a brass input electrode. The inner and outer spheres were separated by a 10-mm (14-mm for the 13-inch) thick nylon insulator with convoluted edges to impede surface flashover. The input electrode was threaded into the center sphere as shown.

Current viewing resistor

On the opposite side of the apparatus a current viewing resistor (CVR) and electrode tip penetrated the cavity between the spheres. The protruding electrode tip promoted discharge through the CVR* which was connected the rear of the tip. For the majority of the experiments a 51.15 mΩ CVR was used. However, to demonstrate that the measurements of the spark characteristics were independent of the CVR a

* T & M Research Products, Series A current viewing resistors: A-5-05, 51.15 mΩ, 2 GHz bandwidth, 180-ps rise time; A-5-2, 204 mΩ, 1.2 GHz, 300-ps rise time.

second CVR with a resistance of 204-mΩ was also used, see “Experiments with a larger (204-mΩ) CVR load” on p. 22.

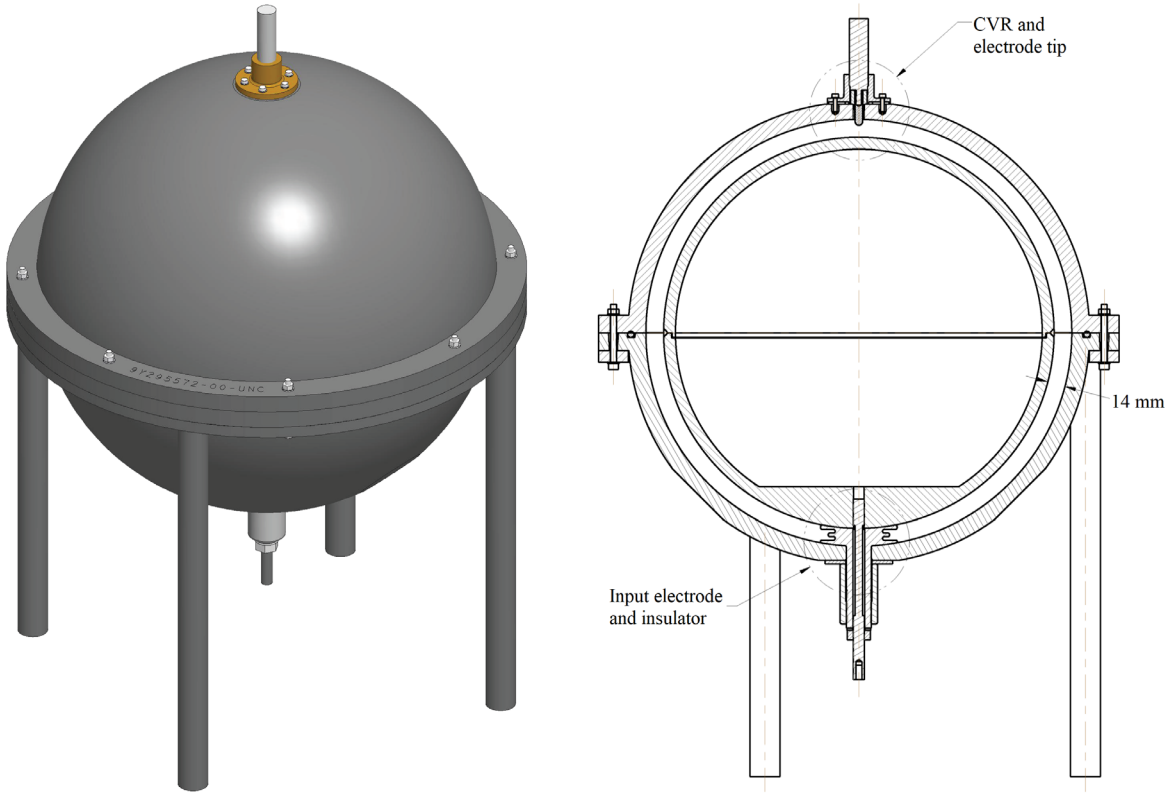

Figure 2. 13-inch apparatus showing the input electrode and convoluted insulator at the bottom, the CVR and electrode tip at the top.

The tip separation from the inner sphere was set manually and this in turn determined the breakdown voltage. The inner sphere was slowly charged via the resistor chain, which was a string of high voltage resistors that were carefully laid out to avoid surface flashover. For the 5-inch apparatus the total resistance of the chain was 120 GΩ, whereas it was 30 GΩ for the 13-inch apparatus.

Elimination of ground loops

The outer sphere was connected to the ground of the high voltage power supply by a pair of 8-MΩ resistors, these effectively isolated an otherwise resonant circuit from ground loops, thus minimizing ringing. With these resistors in place, only the CVR was connected directly to the ground of the digitizer; the digitizer served as the single-point ground of the apparatus. See “Appendix: Prevention of Ground Loops” on p. 38.

Experiments

Concentric spheres

The spark discharge currents for each voltage-gap combination in both 5-in. and 13-in. experiments were recorded, with and without inductance added to the discharge path. The discharges were stochastic, hence 20 experiments per combination were performed, more than a 1600 tests in all, for each voltage-gap combination to obtain reasonable confidence of the mean and standard deviation (SD). At the time of writing, Sept 2019, the 5-in experiments are complete but the 13-in. experiments need additional work on the inductive load experiments; the non-inductive results for the 13-in. are essentially complete and are reported here.

Charging and triggering procedures

To prevent damage to the digitizer equipment, electrode tips and sphere, the concentric spheres were charged via a large charging resistor so that only one discharge would be possible before the spheres would have to be recharged again. The CR time constant of the charging cycle was designed to approximate to 6 seconds[*] so that the voltage on the spheres would be at least 98% of the charging voltage within approximately 30 seconds. In each experiment the charging voltage was adjusted so that there was at least 30 seconds between discharges. The time between discharges would often drift above

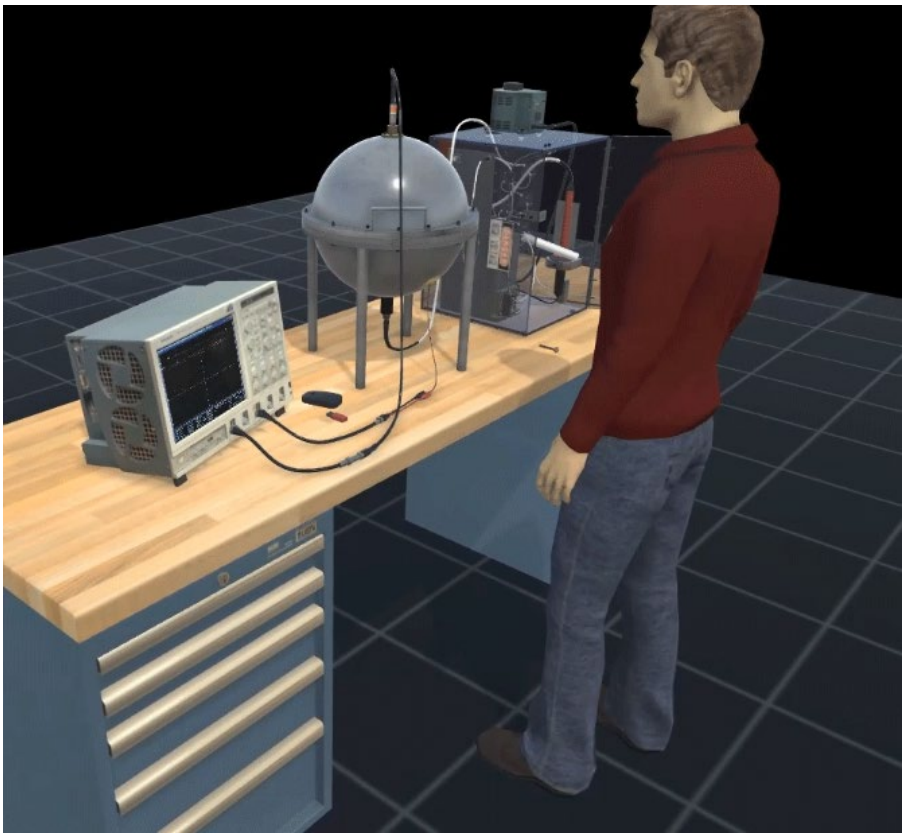

Figure 3. Cartoon of test apparatus. From left to right on the bench: digitizer; concentric spheres of the 13-inch system; and power supply.

[*] Charging resistors of 120 GΩ and 30 GΩ were used to charge the 50 pH and 244 pH spheres.

the 30 seconds and occasionally below it. If the time became too short the charging voltage would be reduced and the series of tests repeated at that lower voltage.

PVDF sensor

The digitizer[*] used to record the current data was triggered either by the current waveform itself or by the signal from a polyvinylidene difluoride (PVDF) piezoelectric sensor,[†] attached to the outer grounded sphere with a thin smear of vacuum grease. The PVDF sensor performed more as a capacitive pickup sensor than a piezoelectric one; it was sensitive to electrical discharges occurring anywhere within the two spheres[‡]. The PVDF sensor was especially useful for detecting discharges that bypassed the CVR electrode and discharged between the two spheres instead; this typically happened when the voltage exceeded the breakdown strength of the air gap between the spheres and around the gap insulator. The PVDF trigger method was found to be superior to self-triggering, because of its consistent magnitude and rapid rate of rise, and was used for the majority of the experiments.

Inductance in the discharge path

The concentric spheres and diagnostics had a negligible inherent inductance, which was originally estimated to be less than 5 nH, see below, whereas in most accident scenarios there will be an inductive component to the discharge path of 100 nH to 1 µH or more. Moreover, in the UK Atomic Weapons Establishment (AWE) drop-ball experiments [2] there was a ground lead attached to the dropping ball; the AWE researchers estimated that the lead had an inductance of at least 220 nH.

New estimate of inherent inductance

After this report had been completed, and thanks to communications with Prof. Durfee from the Colorado School of Mines, this 13-inch sphere inductance was revisited. It is more likely to be 65 nH than the estimated value quoted above.

To determine the effects of the added inductance, external inductances were deliberately added[§] to the discharge paths in these sphere experiments. Only the results of the 5-in. experiments with inductance had been completed at the time of writing, see “Effect of load inductance” on p. 24.

[*] Tektronix DPO 7254C

[†] TE Connectivity LDT1-028K piezo sensor

[‡] The “grounded” outer sphere was isolated from true ground by 8 MΩ to prevent ground loops, see Prevention of Ground Loops on p. 26.

[§] Coaxial cable inductor design, p. 22

Results

In this section the results are captured graphically. The original data may be found in “Appendix: Spreadsheets of 5-inch and 13-inch sphere data” on p.32.

Breakdown voltage versus sphere-to-electrode gap

For both sizes of spheres the breakdown voltage was plotted against the tip to sphere separation, the results are shown in Figure 4. The breakdown voltage was found by slowly adjusting the applied voltage until self-breakdown occurred from tip to inner sphere every 30 seconds. Breakdown was detected by observation of the signal from the PVDF probe.

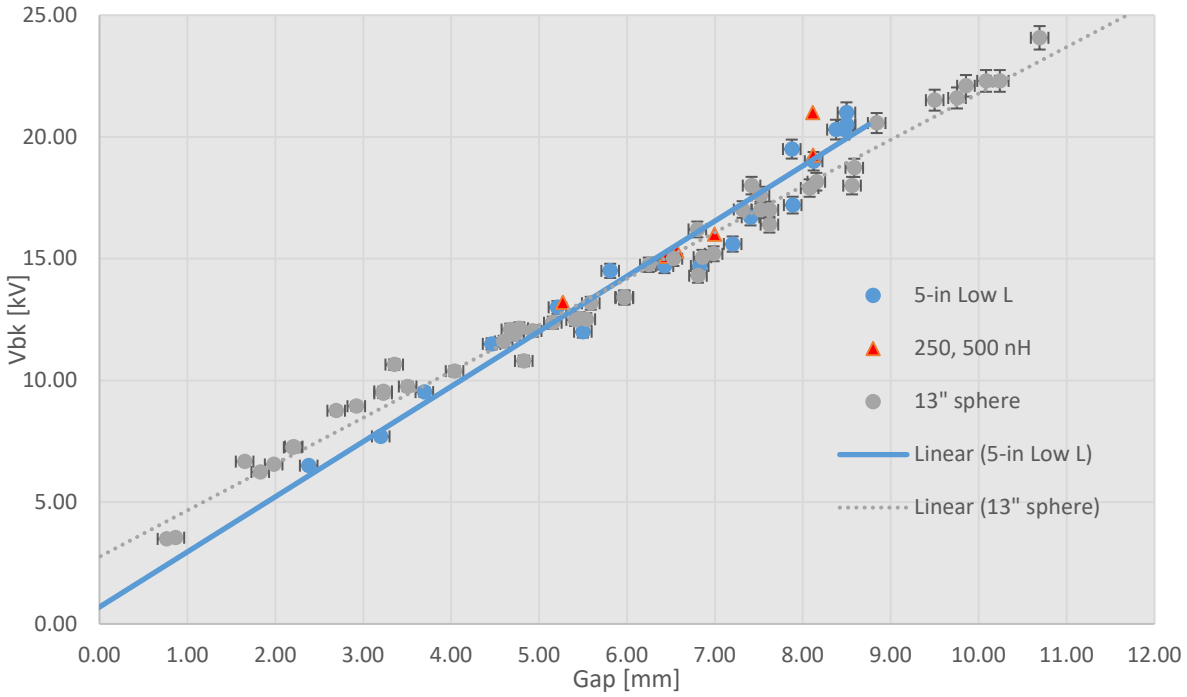

Figure 4. Breakdown voltage in kV versus sphere-to-electrode gap in mm for both the 5-inch and 13-inch spheres. The 5-inch data for the inductive loads are also shown.

As to be expected, there was a linear relationship between the gap and breakdown voltage for both sizes of sphere. The voltage intercept of the 5-inch data for a zero gap was indistinguishable from the origin (0.69 kV with a 95% confidence range of -0.81 to 2.19 kV) but the 13-inch data extrapolated to 2.76 kV at zero gap (95% confidence range 2.30 kV to 3.21 kV); the 13-inch data clearly did not extrapolate through the origin.

The slopes of the two plots were 2.26 kV/mm (95% confidence range 2.04 – 2.49 kV/mm) for the 5-inch data and 1.90 kV/mm (95% confidence range 1.83 – 1.97 kV/mm) for the 13-inch data. [At the altitude of the Los Alamos building where the work was performed (~7500 feet or 2286 m above sea level), the

dielectric breakdown strength of air is estimated to be 2.36 kV/mm from Paschen's law for planar electrodes at 20°C in dry air.][*]

Possible causes of the large intercept in the 13-inch data plot are systematic errors in the gap measurement and field non-linearities due the curvature of the electrode tips and relatively sharp machined edges in the aluminum spheres near the electrode. These non-linearities may also lead to high electric field concentrations and therefore premature breakdown.

Data analysis techniques

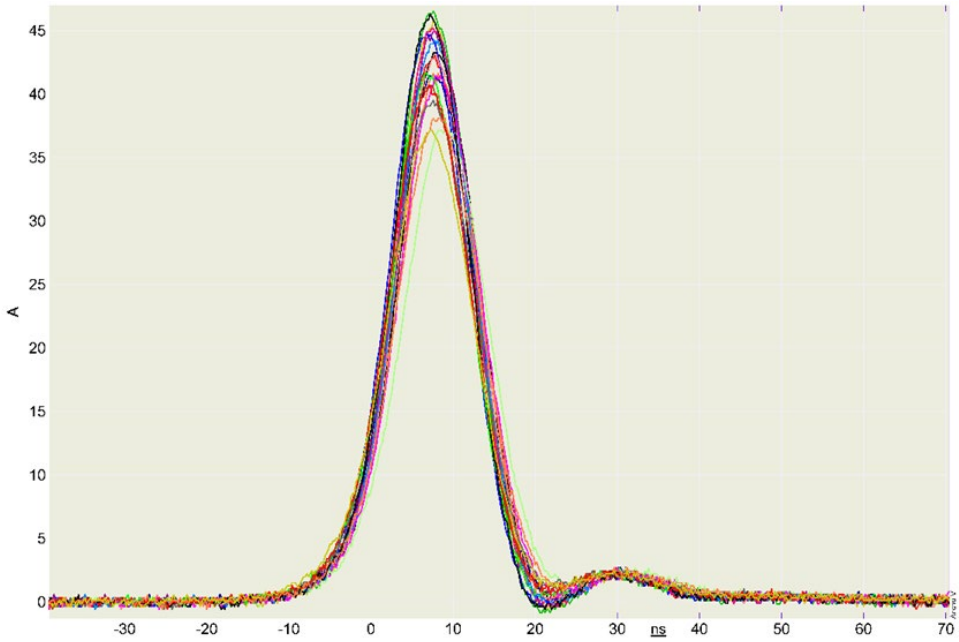

Figure 5. Current profiles [A] of 20 experiments recorded in region 1 for the 5-inch spheres plotted versus time [ns]; applied voltage 9.5 kV, 3.7 mm gap. The peaks range from 37 to 46 A.

In the ensuing presentation of results the data have been analyzed in a uniform process. The current data were recorded as voltages across the CVR; these data were converted to currents from the calibrated CVR resistance value as functions of time *i(t)*, see for example Figure 5; the currents were integrated (numerically) in time to calculate charge transferred to the CVR load Q_{tfr}; the current data were squared to find the power delivered in the CVR load; and those powers were integrated in time to determine the net energy dissipated in the CVR load, E_{cvr}.

For a typical sample of 20 experiments at a given gap and voltage the mean and standard deviation of the peaks were found. The transferred charges, Q_{tfr}, could then be compared with the initial charge, Q_{init} which is the applied voltage V_{brk} multiplied by the estimated capacitance of the spheres.

[*] In these experiments only the temperature of the apparatus and the humidity in the building were recorded. There was no attempt to measure the pressure or humidity within the spheres.

$$
\begin{aligned}
Q_{tfr} &= \int_{-\infty}^{\infty} i.dt \\
E_{cvr} &= R_{cvr} \int_{-\infty}^{\infty} i^2.dt \\
Q_{init} &= CV_{brk}
\end{aligned}
\tag{1}
$$

The above calculations and plots were performed using in-house software [3] and independently verified using Matlab [4].

No detectable progression of data within each series

The spheres remained sealed for all the 20 experiments for each gap-voltage combination (called a series). So there was a possibility that the temperature and pressure of the air within the spheres would increase as the discharge energies (mJ) were deposited from experiment to experiment. Moreover, the gas composition might change as the byproducts of air breakdown and electrode erosion accumulated over the series. Consequently, there was concern that the breakdown characteristics would progressively change throughout each series.

However, in all of more than 60 series (and 1200 discharges) that were performed there was no evidence of a progressive change in the results. The magnitude of the discharge currents from one experiment to the next was stochastic without exception and there was no apparent drift in the results.

Discharge currents versus sphere-to-electrode gap lengths

The results are summarized in the spreadsheets on p. 32 and the complete set of mean peak currents versus the inner sphere-to-electrode gap lengths are presented in Figure 6.

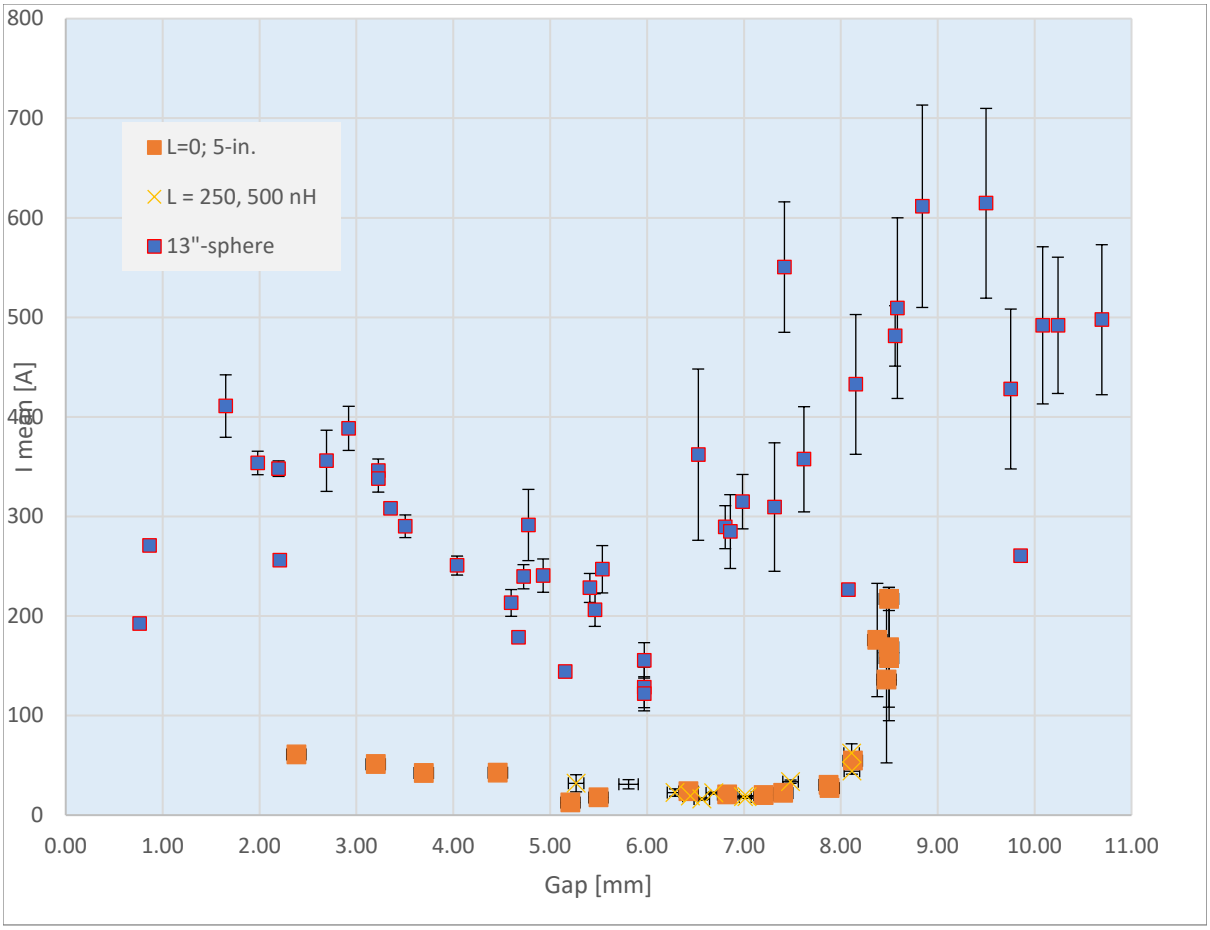

Figure 6. Mean peak currents [A] vs gap lengths [mm] with standard deviation error bars for all experiments on both the 5-inch and 13-inch spheres.

5-inch spheres, two-region behaviors

Starting with the 5-inch spheres, the data at the bottom of the Figure 6 show the mean peak current monotonically decreasing with increasing gap length (hence increasing charge voltage) from a peak of 61 A at 2.38 mm down to a gap of 6.45mm where the current is 19 A. Then above ~7.5 mm the current climbs abruptly to a mean of 217 A at a gap of 8.5 mm. The discharge behaviors before and after 7.5 mm appear to fall into two Regions, 1 and 2.

In Region 1 the peak currents fall with increasing gaps and there is a relatively small variance in the peak currents. The spread of currents is shown in Figure 5 for Region 1 where there is a typical standard deviation of just 2.5 A or 7.6% of the mean.

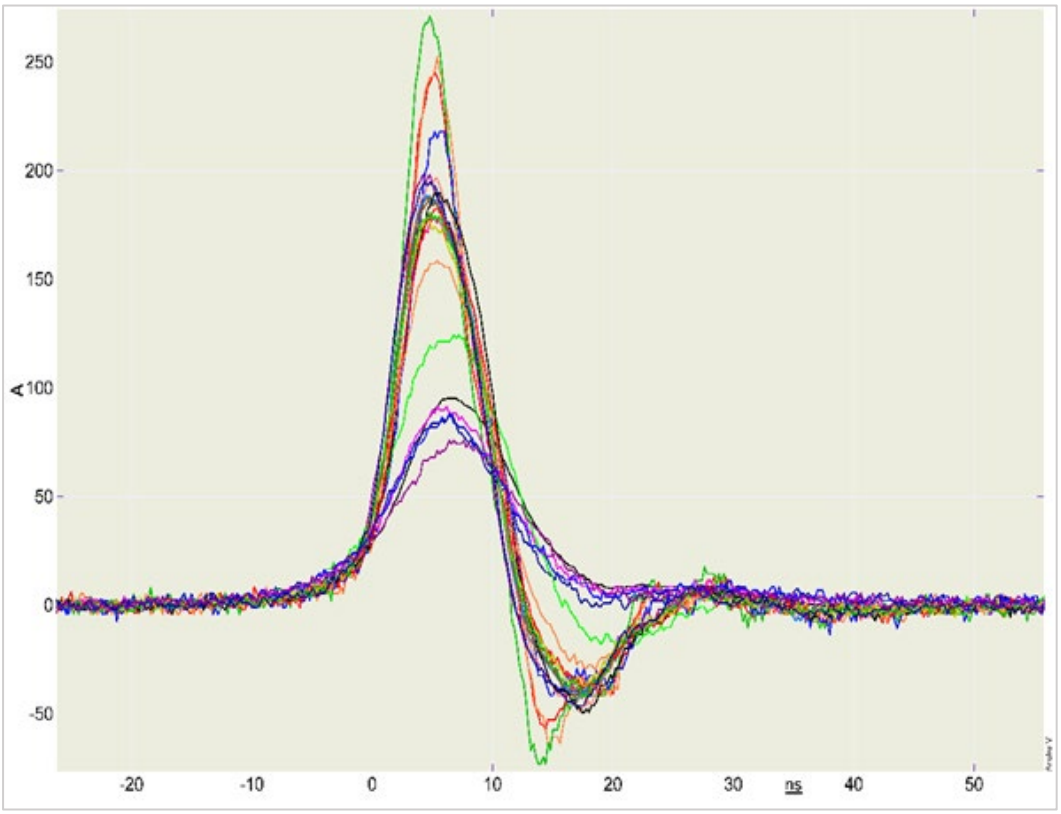

Figure 7. Current profiles [A] of 20 experiments recorded in Region 2 for the 5-inch spheres plotted versus time [ns]; applied voltage 20.3 kV, gap 8.4 mm. The peaks range from 74 to 271 A.

In Region 2 the current increases rapidly with gap and the spread of peak currents is much larger, see Figure 7. The standard deviation is typically 66 A or 32% of the mean, i.e., more than four times larger than for Region 1. Moreover, the peak currents are five times larger in Region 2. The oscillatory nature of the Region-2 behavior will be discussed on p. 25.

A possible explanation for the differences between the two Regions is the available input energy per unit length of gap. The transition from Region-1 to -2 behavior coincides with a minimum energy per unit length of gap of ~1 mJ/mm; this may be the minimum energy required to ionize a self-sustaining discharge channel. This will be discussed further in "Possible minimum energy density for ionization" on p. 19.

Returning to Figure 6, the 5-inch data with inductance are also shown. The peak currents are indistinguishable from those obtained with near zero inductance. The effect of inductance will become more apparent when the deposited energies are examined, "Effect of load inductance" p. 24.

13-inch spheres data

Returning to Figure 6, the mean peak currents versus gap for the 13-inch spheres were an order of magnitude larger than those of the smaller spheres. This is not surprising because the capacitance of the 13-inch system was five times larger than that of the 5-inch spheres, hence the available energy was five times larger.

In these experiments there was no clear two-region behavior. (There may be a downward trend between 3 and 5mm but the scatter in the data make such conclusions of low confidence.) This Region-2 like behavior may be because the available input energy per unit gap length was always >1 mJ/mm for the 13-inch experiments. Recall that from the 5-inch experiments, ~1 mJ/mm appeared to be the minimum energy density necessary to transition from Region 1 to Region 2. Again, this will become obvious in the presentation of energies, in "Energy plots" below.

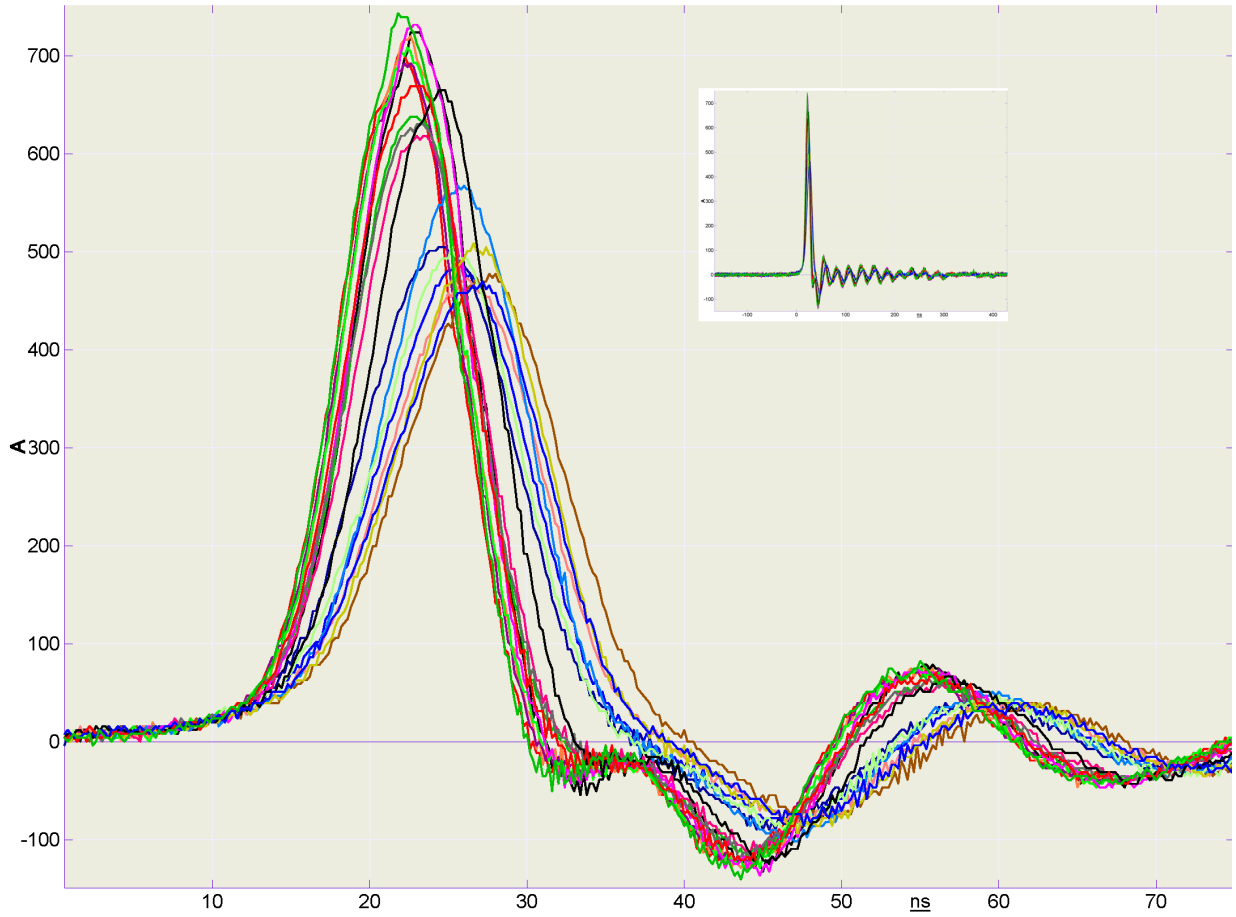

Figure 8. Current profiles [A] of 20 experiments recorded for the 13-inch spheres plotted versus time [ns]; applied voltage 20.57 kV, gap 8.84 mm. The inset is the same data plotted on a longer timescale illustrating that the tails of the signals continue for 300 ns.

Charge conservation as test of full discharge

To ensure that *all* the discharge energy was garnered by the CVR (i.e., none was lost to parallel discharges bypassing the CVR) all the digitized current traces were numerically integrated with time. If the discharge was confined to the tip and nowhere else then the current integral, i.e., the charge delivered to the load, would equal the original charge on the spheres, i.e., electric charge would be conserved.

$$Q = \int_0^\infty I.dt = CV$$

Load charge exceeded source charge

When the integrated currents were compared with the calculated charge (*CV)*, i.e., the estimated capacitance multiplied by the measured charge voltage, they always *exceeded CV* by between 5% and 10%. The cause of this error is unclear.

The voltage probe, used to measure the charge voltage for the capacitor (*V*), was certified by the LANL calibration services to be accurate to within the manufacturer's specification of 2%; and that of the digitizer used to monitor current to within 1%. Moreover, the measured voltages were likely higher than the actual charge voltages because a large charging resistor was used, p. 9. From the charging time we estimated the true charge voltages were ~98% of the measured values.

The error could be due to an underestimate of the capacitances of the spheres or an inaccuracy of the CVR resistance value. The capacitance was calculated from the known dimensions and also measured with a capacitance meter[*]. These values were in close agreement, the meter measured 244 pF ± 6 pF and the capacitance calculated from dimensions was 241 pF (ignoring the capacitance of the supporting plastic insulator, which was estimated to be 4.5 pF).

The CVR is a four-terminal device so contact resistances can have no effect on the internal resistance value used to measure current. The CVR is specified to have been calibrated by Kelvin bridge to an accuracy of 0.2 %, but this is clearly not a high frequency measurement so there may be high frequency errors.

When the experiments were repeated with a larger CVR value, see Experiments with a larger (204-mΩ) CVR load on p.22, it was noted that the charge transfer was closer to 100%, so the smaller CVR value may be in error.

Nonetheless, there was never any apparent loss of charge so we can be certain that all the discharge energy was detected by the CVR.

Adequacy of CVR bandwidth

The 51.15-mΩ CVR had a specified bandwidth of 2 GHz whereas the spectrum of the fastest measured current data decreased monotonically from DC so that it was 40 dB below the DC value at 200-MHz, which was the noise floor of the data. Consequently, provided that the specified bandwidth of the CVR was correct, the measured currents were not perturbed by the bandwidth of the CVR. As a check for a

[*] GLK Instruments, Model 3000, Digital capacitance meter.

possible bandwidth limitation, a 2-GHz miniature Rogowski coil was added in series with the CVR [5]. There was no significant difference between the current data from the two sensors.

Energy plots

As in Eq.(1) the current data were squared and multiplied by the CVR resistance to determine the load powers, then integrated to obtain total energy deposited in the load. The energies deposited in the 51-mΩ load are shown in Figure 9. Clearly the 13-inch sphere data dwarf the 5-inch data, with mean energies approaching 150 µJ. From these data there appears to be a two-region behavior in the 13-inch data where the deposited energy increases significantly above a gap of 6 mm. However, plotting the deposited energy vs. the input energy per unit length is more revealing, see Figure 11.

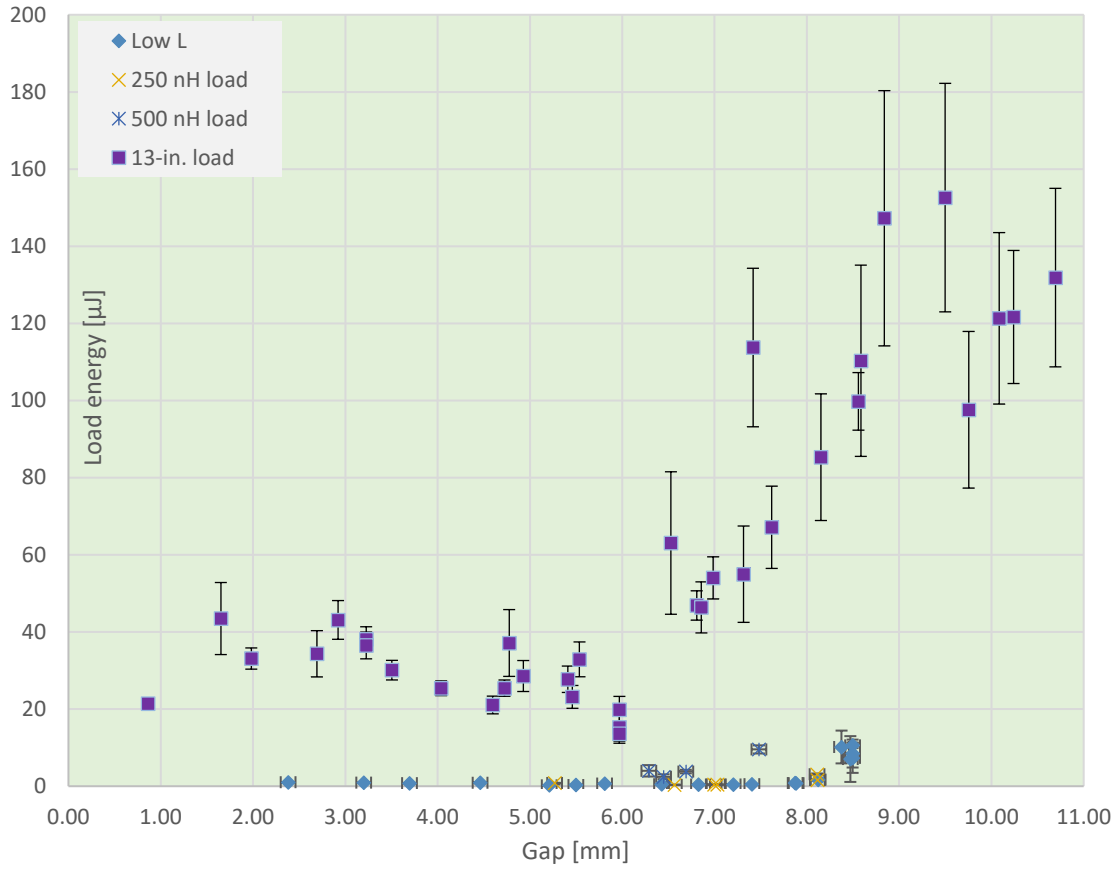

Figure 9. Mean load energies [µJ] deposited in the 51-mohm CVR versus gap [mm} for both the 5-inch and 13-inch spheres. The inductive load data is included for the 5-inch spheres. The error bars indicate one standard deviation (SD) σ from the mean.

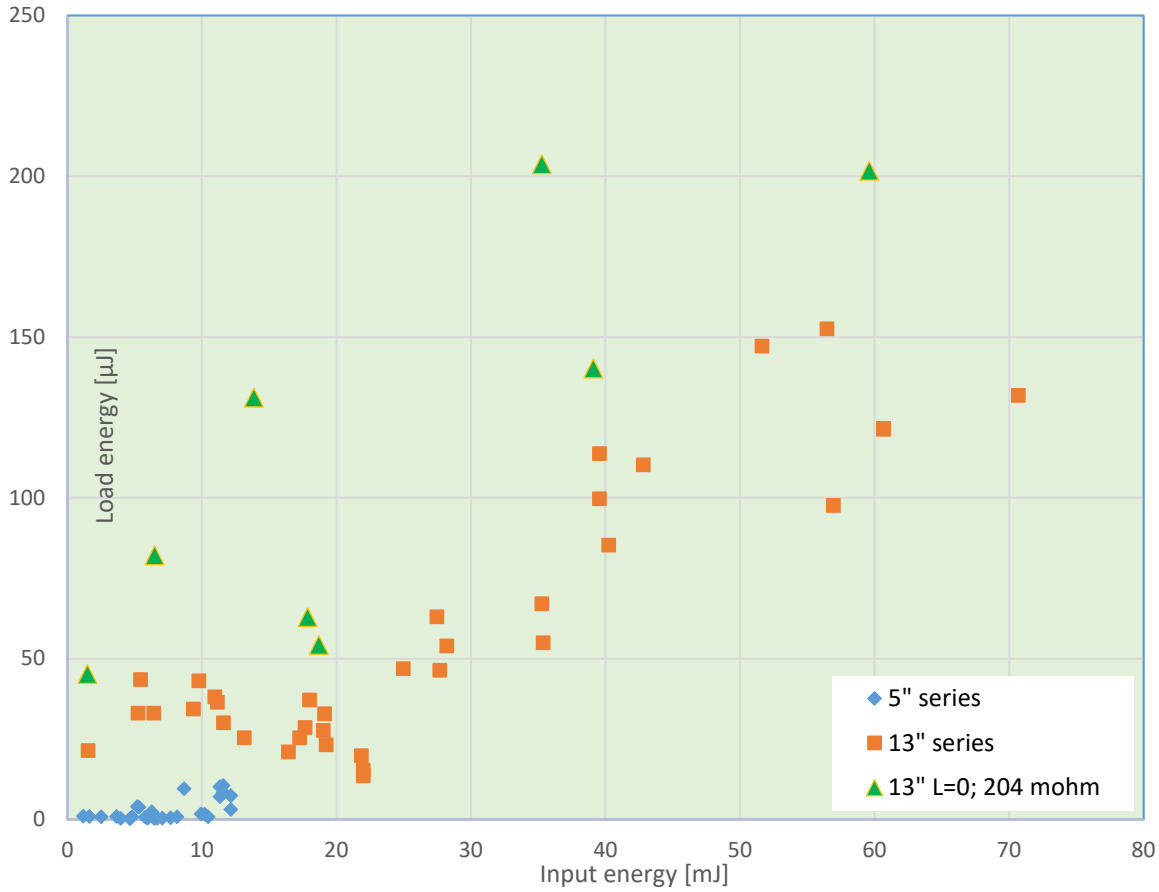

Figure 10. Load energies [µJ] versus input energies [mJ] for the 5-inch and 13-inch spheres with two load resistors. The 5-inch data used only the 51.15-mΩ load, the 13-inch data include the results for both the 204-mΩ and 51.15-mΩ loads.

Plotting input versus output energies, Figure 10, shows all the data for the two sphere sizes and the effects of changing the load resistances; the effect of load resistance is discussed later in "Equivalent spark resistance" on p. 21.

Possible minimum energy density for ionization

Figure 11 reinforces the observation that there is a minimum energy per unit gap length (energy density) of 1 mJ/mm necessary to deposit significant energy into the load. (As conjecture, approximately 1 mJ/mm may be the energy density necessary to sufficiently ionize and sustain spark channel growth.) The behavior of the data also suggests that there may be an upper bound to the energy deposited that is a function of gap. To continue that analysis the load energy density (i.e., per unit length) has been plotted in Figure 12. In that presentation of the data the conclusions are largely the same although the necessary minimum energy density for sustained spark growth and energy deposition appears to be closer to 1.5 mJ/mm than 1.0 mJ/mm.

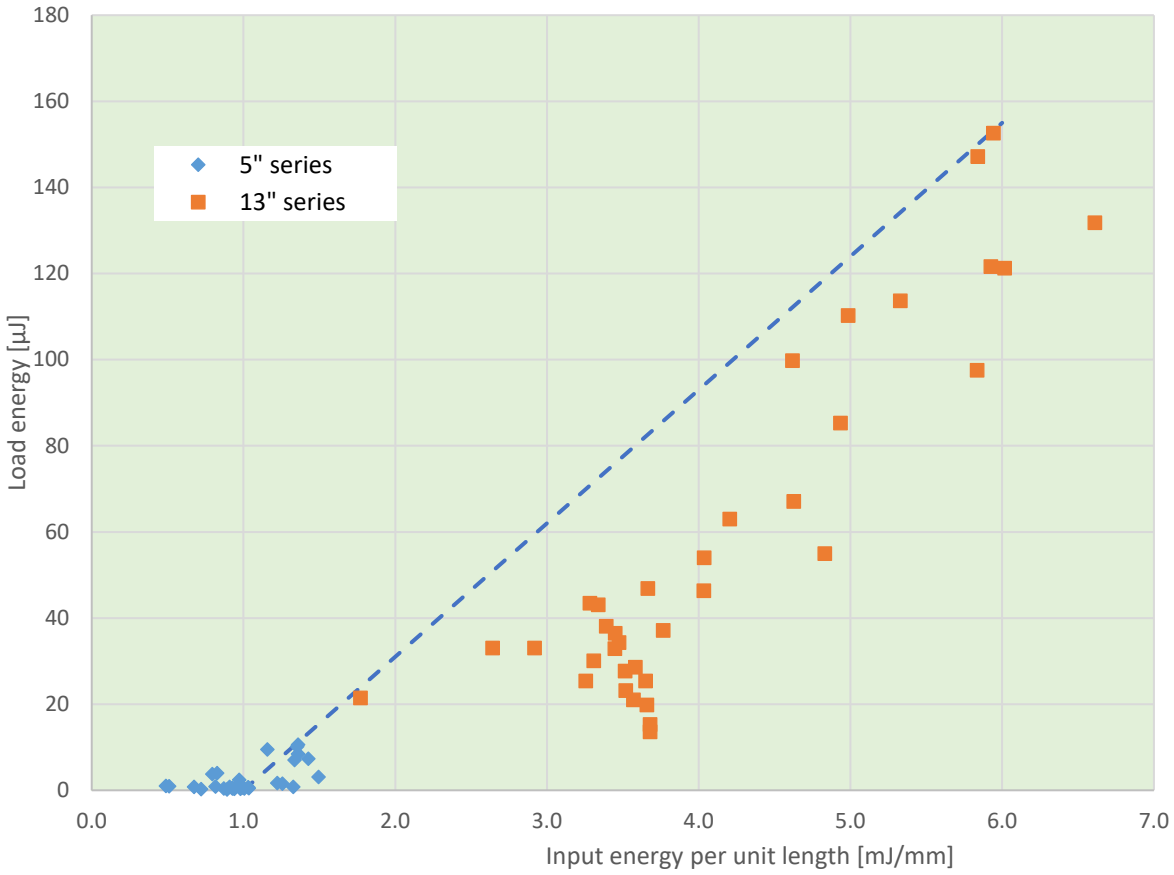

Figure 11. Mean load energy [µJ] deposited in a 51-mohm CVR load vs. input energy per unit gap length (energy density) [mJ/mm] for the 5-inch and 13-inch spheres. The dashed line suggests a possible upper bound to the deposited energy as a function of input energy density above ~1 mJ/mm.

Ratio of input to load energies in worst case

From both the dotted line in Figure 11 and the upper bound of Figure 12 it appears that the maximum energy transfer efficiency, from stored electrostatic energy to deposited Joule heating, is approximately 1.5% for the 51-mΩ load. For other load resistances the deposited energy scales with resistance, see p.23.

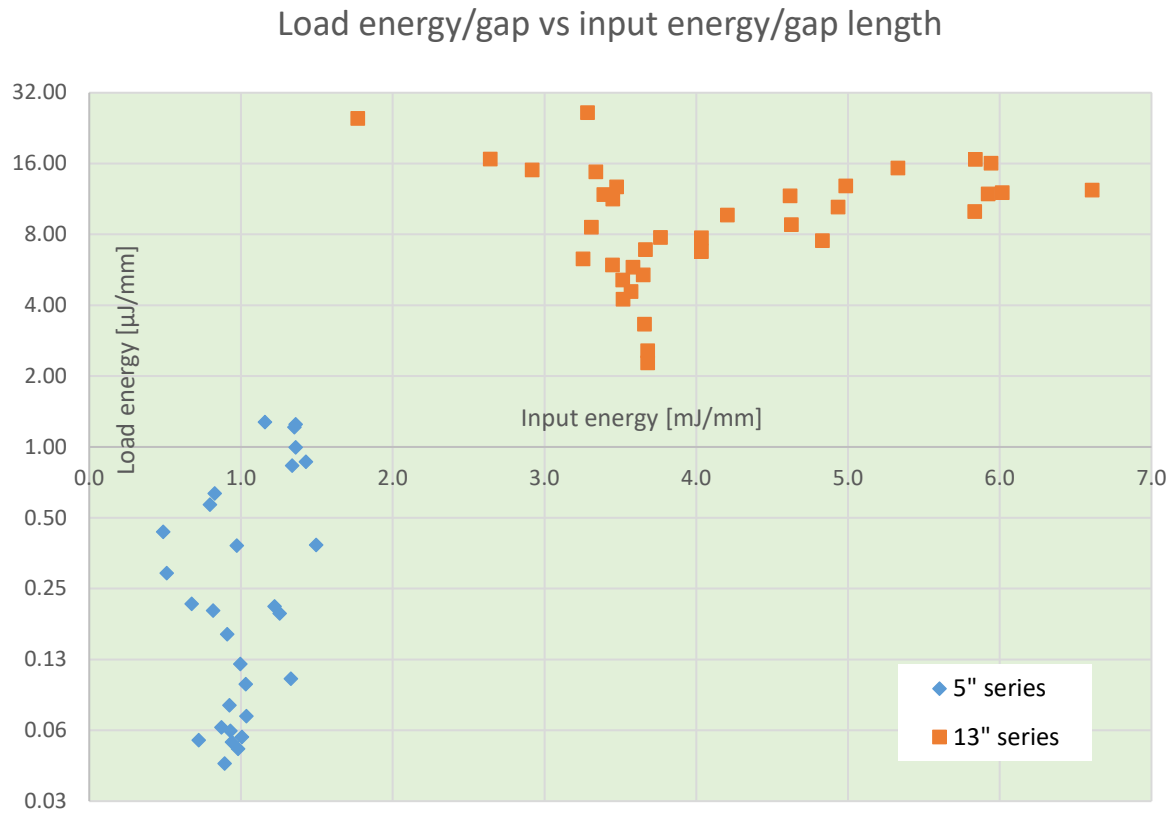

Figure 12. Mean load energy density [µJ/mm] deposited in a 51-mohm CVR load vs. input energy per unit gap length (energy density) [mJ/mm] for the 5-inch and 13-inch spheres on a log-log plot.

Equivalent spark resistance concept

Clearly from Ohm's law, the energy deposited in the CVR load is a function of its resistance as well as the remaining energy available after creation of the spark. One method of scaling the results to any load is to calculate an equivalent (time independent) spark resistance that would deposit the same energy as that measured in the load. We can define this equivalent spark resistance, R_{spk}, by equating the energy stored in the spheres to the total energy dissipated in the spark and the CVR load. Then we rearrange to determine the equivalent resistance.

$$E_{sph} = \frac{1}{2} C V_{bk}^2 = \int i^2 dt.(R_{spk} + R_{cvr})$$
$$R_{spk} = R_{cvr}\left\{\frac{E_{sph}}{E_{cvr}} - 1\right\} \quad (2)$$

Here V_{bk} is the voltage between the spheres at breakdown, E_{sph} is the energy stored in the spheres, and E_{cvr} is the energy deposited in the load. By defining the equivalent spark resistance the results become

independent of the CVR resistance. As will be seen on p. 23, the CVR resistance has a weak influence on spark formation and the spark may be considered to be a constant current source.

Experiments with a larger (204-mΩ) CVR load

The results shown in Figure 12 have been replotted to include the data for a 204-mΩ CVR load in Figure 13. As to be expected, the deposited energy was higher because of the four-fold increase in resistance. From the considerations of equivalent spark resistance below we find that this behavior is predictable.

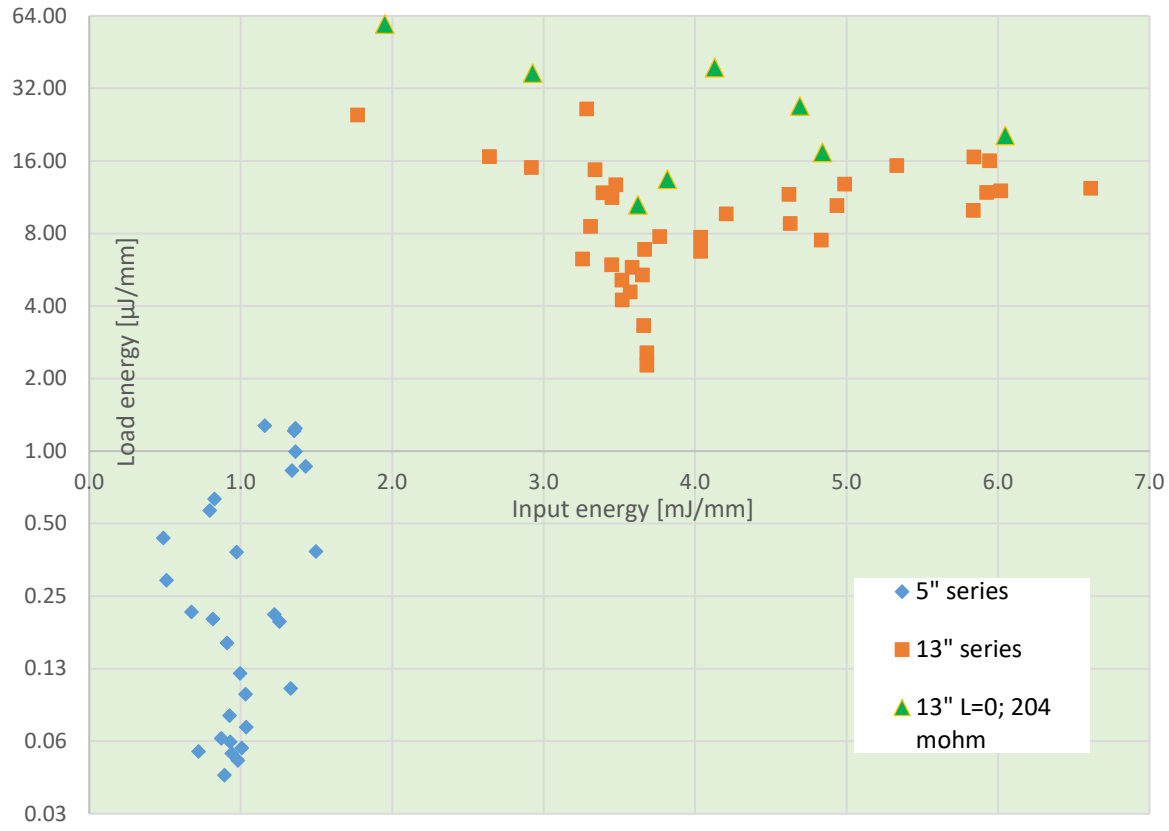

Figure 13. Replot of Figure 11 with the energy data for a 204- mΩ load added. Mean load energy density [µJ/mm] deposited in 51-mΩ and 204-mΩ CVR loads vs. input energy per unit gap length (energy density) [mJ/mm] for the 5 inch and 13-inch spheres on a log-log plot.

Equivalent spark resistances

Using Eq(2) the equivalent spark resistances have been plotted as a function of input energy, Figure 14. By combining the data for both values of CVR resistances into equivalent spark resistance calculations the results show that the equivalent resistances for the larger CVR are comparable to the smaller CVR but slightly higher. The larger load resistance reduces the current in the spark, thereby reducing the ionization and expansion of the spark channel. Hence the resistance of the spark is increased.

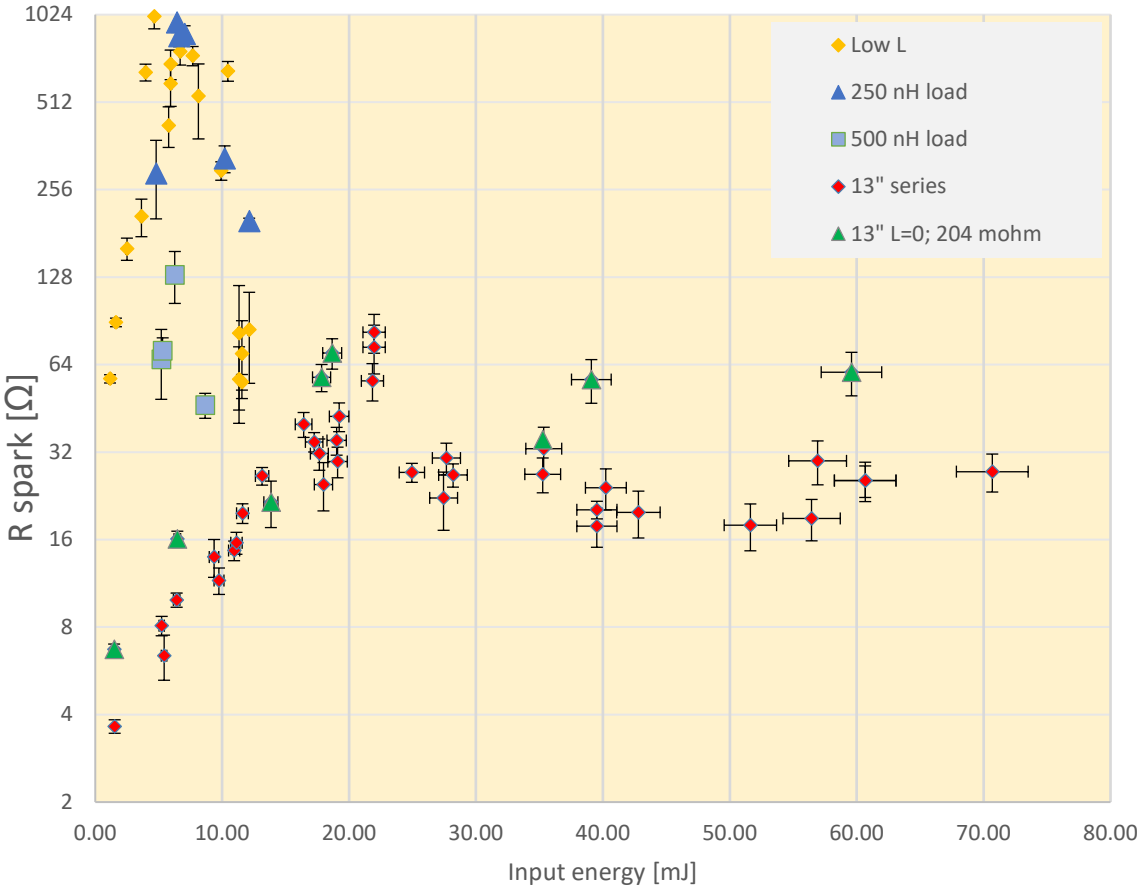

Figure 14. Log-linear plot of the equivalent spark resistance [Ω] versus input energy [mJ] for the 5-inch (with and without inductance) and the 13-inch spheres, with 51-mΩ or 204-mΩ CVR loads. The error bars represent 3-σ deviations from the means.

Spark behaves as a constant current source

The significance of the spark resistance plot is that the effective spark resistances are many orders of magnitude larger than the likely load resistances. For example, a common resistance of an exploding bridgewire (EBW) detonator is 19 mΩ* whereas the measured spark resistances in the figure are typically tens of Ohms. This is important because we can thus treat the spark as a constant current source, i.e., to a first approximation the spark current is independent of the CVR load resistance. Hence the action integral, $\int i^2 dt$, is also independent of load . Consequently for a given source the energy dissipation in the load is directly proportional to the load resistance. For example, with the 13-inch spheres the maximum deposited load energy would be $E_{13} = 2.93 \times 10^{-3} R_{cvr}$ [J] for load resistances up to a few Ohms.

* For a gold bridgewire, 38.1 µm diameter, 1 mm long at room temperature

Effect of load inductance

As mentioned earlier, in many accident scenarios and ESD experiments there is a finite inductance in the discharge path. For example, it was estimated by AWE researchers that their drop-ball tests had an inductance of at least 220 nH in the circuit. In the experiments described below, inductances of 250 nH and 500 nH were added to the load (CVR) circuit. Theoretical calculations of the inductive effects, based on the Braginskii model, compare favorably with the experimental results, see p. 35.

Coaxial cable inductor design

5-inch sphere, spark duration limitation

For relative ease of construction a coaxial inductor design was chosen. A short-circuited* coaxial cable behaves like an inductor, provided that the duration of the signal (in this case the spark discharge) is long compared to the round-trip transport time in the cable. In the case of the 5-inch sphere data the current durations were typically >50 ns and the long-duration condition was satisfied. (As will be see, this condition was not met with the 13-inch data.)

Two inductance values were chosen, 250 nH and 500 nH and these were simulated by using 1-m and 2-m lengths of type RG214, 50-Ω coaxial cable. RG214 was chosen because of its low DC resistance (9 mΩ/m). For these two lengths of cable the round-trip times were 10 ns and 20 ns respectively, i.e., short enough compared to the signal durations.

Discharges in the 13-inch sphere violated the spark duration limitation

As was discovered later in the experimental program, the spark currents in the 13-inch experiments were shorter in duration (and an order of magnitude larger) so the cable lengths were consequently too long for them to behave like inductors. The cables loaded the short duration signals with their pulse impedance (50 Ω), rather than the CVR load, and the instantaneous voltage across the cable exceeded the electric breakdown strength of the connections. For example, a typical discharge of 400 A would create a voltage of 2 kV across the connector to the 50-Ω cable and electrical breakdown would occur without adequate insulation. Consequently, the inductors and cable connectors were redesigned for the 13-inch experiments. These modifications were performed too late to be reported here.

* The 51-mΩ CVR approximates to a “short-circuit” in this instance.

Discharges in 5-inch apparatus with cable inductance

The added inductance had a clear effect on the discharge. For the discharge into negligible inductance (i.e., the inductance of the spheres) a single discharge pulse was observed. In the case of the added inductance the discharge was oscillatory, as shown in Figure 15.

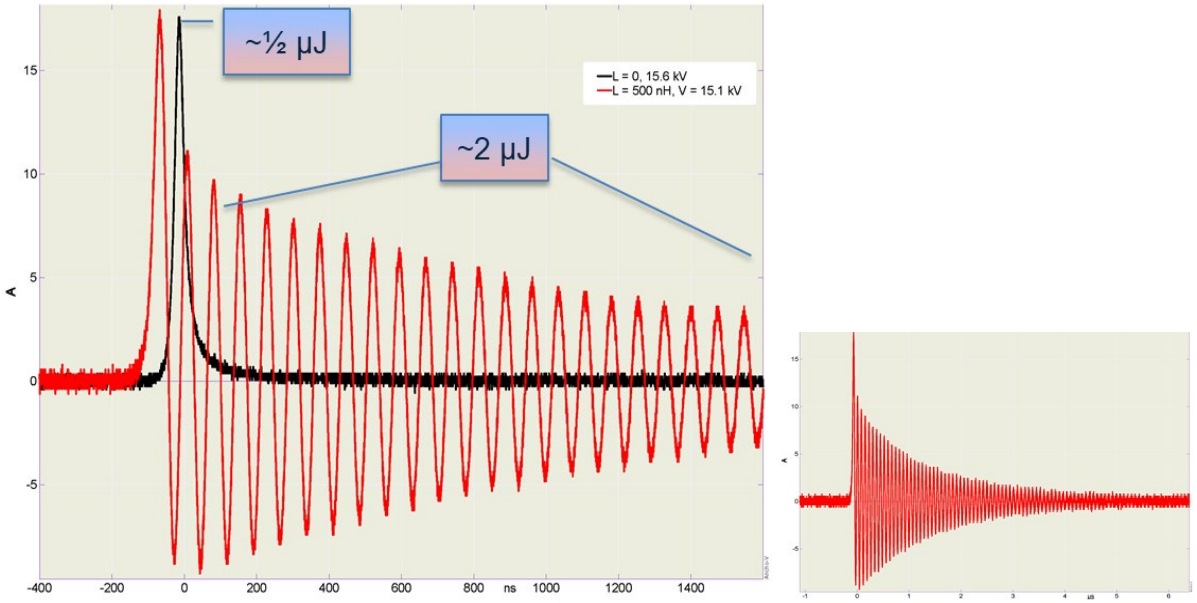

Figure 15. Left: Two current discharges in the 5-inch apparatus, one with and one without a 500-nH included inductance; 51-mΩ CVR load. The single pulse is a 15.6-kV discharge into a negligible inductance. The oscillatory waveform is a 15.1-kV discharge into 500 nH. The small plot on the right shows the same oscillatory signal on a longer time scale of -1 to 8 µs.

In the left of the figure the data of two nearly identical experiments were chosen for comparison, the first without inductance and the second with 500 nH added. The duration of the low inductance discharge was approximately 100 ns (10% peak to 10% peak) with a peak 17.6 A[*], whereas the 500-nH discharge had a duration of ~5 µs with a peak of 17.7 A.

Energy transfer with Inductance

Although the peak currents and peak powers (15.8 W and 16.4 W) of the two discharges were nearly equal the current duration had a significant effect on the energy deposited in the CVR. (In all the experiments performed the inductance had no effect on the peak currents or powers.) In the low inductance experiment the energy deposited was 409 nJ compared to 2 µJ for the 500-nH test. Clearly, *the inductance of the circuit can have a significant effect on the energy dissipated in the load*. As will be seen in Figure 16, the increase in inductance does not always result in an increase in energy dissipation. The inductance apparently makes the most difference in the transition between region 1 and region 2 behaviors, i.e., when the spark channel is only partially ionized. The increase in energy deposition is not apparent for the 250-nH load but for the 500-nH the energy deposition has increased by an order of magnitude in the vicinity of the transition region between 6 and 8 mm.

[*] Low inductance: Shot 1, 15.6 kV, 1/26/2018. 500 nH: Shot 1, 15.1 kV, 10/25/2018

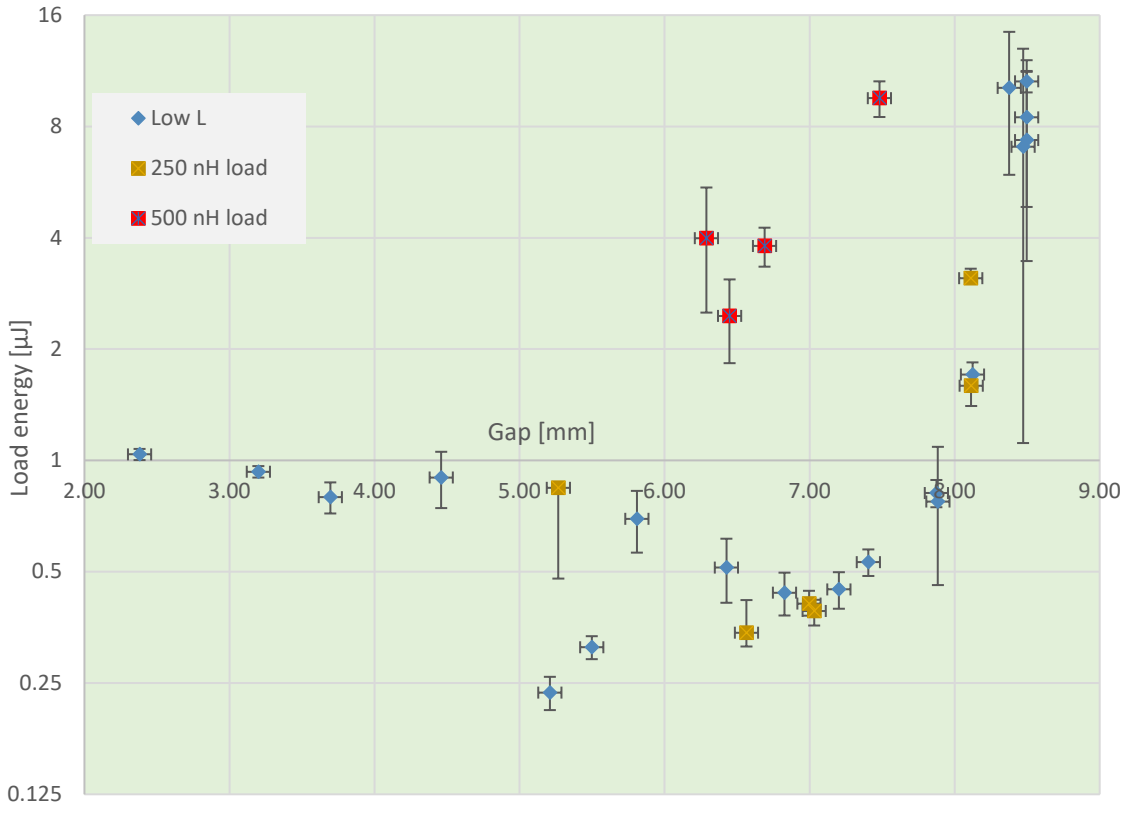

Figure 16. Load energy [µJ] (log scale) vs. gap [mm] for the 5-inch spheres, with low inductance, 250 nH or 500 nH. Error bars are one σ from the mean.

Data Summaries

5-inch sphere data summary

The 5-inch sphere apparatus had a capacitance of 52 pF and the maximum voltage that it could withstand was 21 kV; above that voltage, breakdown would occur directly between the spheres, thus bypassing the gap between electrode-tip and the center sphere. Consequently, the maximum input energy in this 5-inch system that could be monitored was 12 mJ.

The data showed the majority of the electrical energy was dissipated in the arc and a small fraction, ~0.1% worst case into the 51.15-mΩ load, with or without added inductance. The mean peak discharge current was 220 A ± 12 A* and the maximum load energy (into 51-mΩ) was 10.6 μJ ± 2.1 μJ† (0.092% of input energy, 11.5 mJ). The discharge energy for any relatively small resistance was also found, see p. 23.

Estimates of load energy, for any small load

The lowest observed equivalent arc resistance was 55 Ω ± 16.8 Ω† which is orders of magnitude larger than the likely load, so the load current was found to be (to a first degree approximation) independent of the likely load resistance, R_L. Up to $R_L \approx 1\ \Omega$, the maximum energy deposited in the load would be $R_L \int i^2 dt$, i.e., the action integral times the load resistance, here $\int i^2 dt \equiv 207\ \mu J/\Omega$. Even for the relatively large 1-Ω load resistance (compared to a bridge wire resistance of tens of milliOhms) this energy would amount to only 1.8% of the source energy.

Moreover, the ionization and expansion of the spark channel depends strongly on the magnitude of the current, see Braginskii Model, p. 35. Larger load resistances will reduce the current and hence increase the resistance of the spark channel; the 204-mΩ load data of Figure 14 show this effect. Consequently, the 207 μJ/Ω estimate is conservatively low.

Negligible effects of adding load inductance to 5-inch data

Fixed inductances of 250 nH and 500 nH (using coaxial cables) were added to the CVR discharge path of the 5-inch apparatus to determine their effects on the spark energy transferred to the load.

With the exception of the transition regime between regions 1 and 2, the added inductance increased the duration of the current (by up to three orders of magnitude) but had little effect on energy transfer. The equivalent spark resistances appeared to be slightly reduced to 46.5 Ω ± 4.6 Ω†, but given the three-sigma error bars the change was of low statistical significance; we conclude that the energies transferred to the load were not significantly increased. In the transition regime the energy transferred to the load with inductance was increased by an order of magnitude, but the increased energy was less than the energies transferred in region 2, with or without a load inductance.

* ± one standard deviation (1σ).
† ± three standard deviations (3σ).

13-inch sphere data summary

The 13-inch sphere apparatus had a capacitance of 240 pF and the maximum voltage that it could withstand, before breakdown away from the tip, was 24.1 kV. Consequently, the maximum input energy in this 13-inch system was 71 mJ.

The 13-inch sphere data, with low inductance, showed again that the majority of the electrical energy was dissipated in the arc and a small fraction reached the load. The largest transferred energy was 153 µJ into a 51.15 mΩ load, which was 0.27% of the available input energy. The maximum deposited load energy per Ohm was 2.93 mJ/Ω for load resistances up to a few Ohms, compared to 207 µJ/Ω for the 5-inch data.

The mean peak discharge current was 615 A ± 95 A (compared to 220 A ± 12 A for the 5-inch data) but the equivalent spark resistances were 17.8 ± 2.7 Ω (compared to 55 Ω ± 16.8 Ω for the 5-inch data). This 17.8- Ω has the caveat that this is the lowest resistance in the region where there were input energies above 10 mJ. In the lower energy region the effective resistances were lower, see Figure 14.

Conclusions

The magnitudes of the observed spark discharges were stochastic, so more than 1200 tests were required to develop the statistical bounds of the spark behavior, i.e., to estimate the worst case (highest likely) energy depositions in the loads.

5-in. data

For the 5-inch spheres the maximum mean load energy was 10.6 μJ, deposited into a 51.15-mΩ load, with a standard deviation of 0.7 μJ and a sample size of 20. This load energy amounted to less than 0.1% of the input energy $\frac{1}{2}CV^2$. The lowest (most hazardous) observed equivalent arc resistance was 55 Ω which was orders of magnitude larger than the likely victim load resistance. Consequently, action integral of load current is approximately constant and the load energy can be readily scaled to load resistance as $\int i^2 dt$ = 207 μJ/Ω.

A two-region behavior was observed in the 5-inch data. For low applied voltages, the mean peak current decreased monotonically with increasing charge voltage. Then above ~17 kV the current climbed abruptly. The discharge behaviors before and after 17 kV appeared to fall into two Regions, 1 and 2. A possible explanation for the differences between the two Regions is that there is minimum energy required to ionize a self-sustaining discharge channel, and below 17 kV for the 5-inch system there is not enough energy per unit length of discharge.

The added load inductance may slightly reduce the effective spark resistance but the results are not statistically significant.

13-in. data

For the 13-inch spheres the maximum mean load energy was 153 μJ, deposited into the 51.15-mΩ load, with a standard deviation of 30 μJ and a sample size of 20. This load energy amounted to 0.27% of the input energy. The lowest observed equivalent arc resistance was 17.8 Ω. Here again the load energy could be scaled to load resistance as $\int i^2 dt$ = 2.93 mJ/Ω.

There was no obvious two-region behavior in the 13-inch data, probably because there was sufficient energy required to ionize self-sustaining discharge channels in the larger spheres.

Scaling of data to CVR resistance

The resistance scaling was tested by substituting a 204-mΩ CVR for the 51.15-mΩ device. The larger CVR gave comparable but slightly higher effective spark resistances. We conclude that the spark resistances obtained with the 51.15-mΩ CVR are conservative.

Anomaly: Load charge exceeded source charge

When the integrated currents were compared with the calculated charge (*CV)*, i.e., the estimated capacitance multiplied by the measured charge voltage, they always *exceeded CV* by between 5% and 10%. The reason for this discrepancy is unclear but the most likely cause is an error in the value of the CVR resistance, see p.22.

No loss of charge

There was never any apparent loss of charge so we can be certain that all the discharge energy was detected by the CVR.

No evidence of gas contamination or electrode degradation

In more than 60 series of tests (more than 1200 discharges) that were performed there was no evidence of a progressive change in the results. The magnitude of the discharge currents from one experiment to the next was stochastic without exception and no drift in the mean was observed.

Future work

For completeness of the study, future work should include the following.

Charge transfer errors

The errors in charge transfer should be traced (p. 17). Two areas of focus would be an accurate determination of the sphere capacitances and a broad-band verification of the CVR resistances.

13-inch discharges with inductance

The discharge data for the 13-inch spheres should be extended to include inductive loads. To this end a well-insulated inductive load has been designed and manufactured.

13-inch discharges with larger gaps

The 13-inch study should be extended to larger gaps. There is likely some imperfections in manufacture that cause high electric field concentrations. These should be traced and eliminated.

Welding fluid leakage

It was also found that, despite careful rinsing of the interior, fluid tended to leak from the welds of 13-inch inner sphere, both from the inside and outside. When sufficient fluid accumulated on the bottom insulator (Figure 2) the leakage would limit the maximum voltage to 25 kV. The fluid appeared to originate from seepage through pinholes in the weld, i.e., from fluid trapped within the weld.

Table 1. Data for 5-inch spheres.

Gap mm	Vmeas kV	I mean A	SD I A	Mean Load Energy µJ	SD load energy µJ	Mean Load Energy/ gap µJ/mm	Input energy mJ	Input energy /gap mJ/mm	Effective R spark ohm	3*SD Reff ohm	Rspark / gap mm	3*SD Rspark /mm	Charge nC	Calc cap pF	L nH
5.81	14.50	31.02	4.64	0.695	0.132	0.12	5.78	1.00	425.5	67.9	73.2	11.7	840	57.93	
8.50	20.50	217.17	11.65	10.596	0.707	1.25	11.56	1.36	55.7	3.4	6.6	0.4	1200	58.54	
8.50	21.00	157.73	62.88	7.35	3.89	0.87	12.13	1.43	84.3	29.2	9.9	3.4	1240	59.05	
8.50	20.50	168.52	60.08	8.466	3.62	1.00	11.557	1.36	69.8	20.9	8.2	2.5	1300	63.41	
7.88	17.20	27.13	1.37	0.774	0.314	0.10	8.136	1.03	537.6	155.1	68.2	19.7	989	57.50	
3.20	7.70	51.1	1.23	0.9318	0.03326	0.29	1.630	0.51	89.5	3.0	28.0	0.9	467	60.65	
4.46	11.50	42.6	5.95	0.899	0.156	0.20	3.637	0.82	206.9	30.5	46.4	6.8	700	60.87	
2.38	6.50	60.97	1.62	1.038	0.036	0.44	1.162	0.49	57.2	1.9	24.0	0.8	403.5	62.08	
8.12	19.00	54.63	3.62	1.707	0.134	0.21	9.928	1.22	297.4	21.6	36.6	2.7	1166	61.37	
8.47	20.30	136.1	83.61	7.048	5.934	0.83	11.332	1.34	82.2	37.5	9.7	4.4	1278	62.96	
8.38	20.30	175.9	56.90	10.17	4.25	1.21	11.332	1.35	56.9	16.7	6.8	2.0	1309	64.48	
6.83	14.70	20.62	2.29	0.4388	0.05817	0.06	5.942	0.87	692.7	81.0	101.5	11.9	844	57.41	
6.43	14.70	23.73	4.00	0.513	0.101	0.08	5.942	0.92	592.5	97.4	92.2	15.2	850	57.82	
7.20	15.60	19.98	1.79	0.4477	0.0507	0.06	6.692	0.93	764.6	77.7	106.2	10.8	887	56.86	
5.50	12.00	17.67	1.00	0.3123	0.0223	0.06	3.960	0.72	648.5	43.2	118.0	7.9	685	57.08	
3.70	9.52	42.35	2.88	0.7952	0.0767	0.22	2.492	0.67	160.3	14.1	43.4	3.8	570	59.87	
7.40	16.70	22.13	1.44	0.5306	0.04378	0.07	7.669	1.04	739.3	56.3	99.8	7.6	942	56.41	
5.21	13.00	12.61	1.11	0.2355	0.0243	0.05	4.648	0.89	1009.4	94.4	193.8	18.1	724.5	55.73	
7.87	19.50	30.35	1.94	0.816	0.0691	0.10	10.457	1.33	655.4	51.1	83.2	6.5	1077	55.23	
With inductance															
8.11	21.00	62.16	9.50	3.11	0.077	0.38	12.128	1.50	199.4	4.8	24.6	0.6	1200	57.14	250
7.00	16.00	18.27	1.04	0.41	0.0298	0.06	7.040	1.01	878.2	59.5	125.5	8.5	939	58.69	250
6.56	15.30	16.2	1.12	0.342	0.0282	0.05	6.4375	0.98	962.7	73.3	146.7	11.2	890	58.17	250
6.45	15.10	18.95	1.93	2.459	0.627	0.38	6.2703	0.97	130.4	26.4	20.2	4.1	856	56.69	500
7.48	17.75	33.6	1.67	9.54	1.055	1.28	8.664	1.16	46.4	4.6	6.2	0.6	961	54.14	500
8.11	19.25	44.13	2.99	1.592	0.189	0.20	10.190	1.26	327.4	34.7	40.3	4.3	1151.4	59.81	250
5.27	13.20	32	8.60	0.843	0.364	0.16	4.792	0.91	290.7	87.6	55.2	16.6	784	59.39	250
7.03	15.50	18.27	1.34	0.3915	0.0339	0.06	6.607	0.94	863.1	68.7	122.8	9.8	900.5	58.10	250
6.29	13.75	22.69	3.69	3.99	1.48	0.63	5.199	0.83	66.6	18.0	10.6	2.9	785.6	57.13	500
6.69	13.90	22.19	1.06	3.8	0.459	0.57	5.313	0.79	71.5	7.7	10.7	1.1	855.2	61.53	500

Table 2. Sheet 1 of 2, data for 13-inch spheres.

Vmeas kV	Gap mm	I mean A	SD I A	Input energy mJ	Input energy/ gap mJ/mm	Mean Load Energy µJ	SD load energy µJ	Mean Load Energy/ gap µJ/mm	Effective R spark ohm	3*SD Reff ohm	Rspark/ mm	3*SD Rspark/ mm	Charge nC	Calc cap pF
With 51.15 mohm load														
13.38	5.97	155.44	17.80	21.84	3.66	19.864	3.422	3.33	56.2	8.3	9.4	1.4	3678.9	274.96
13.42	5.97	128.31	20.36	21.97	3.68	15.3	3.61	2.56	73.5	14.0	12.3	2.3	3663.8	273.01
13.42	5.97	121.873	17.13	21.97	3.68	13.596	2.45	2.28	82.7	12.6	13.8	2.1	3653.8	272.27
12.03	4.93	240.58	16.73	17.66	3.58	28.57	4.016	5.80	31.6	3.9	6.4	0.8	3363.2	279.57
8.94	2.92	388.48	22.16	9.75	3.34	43.11	5.02	14.76	11.6	1.2	4.0	0.4	2540	284.12
6.55	1.98	353.72	11.79	5.23	2.64	33.1	2.75	16.71	8.1	0.6	4.1	0.3	1834.3	280.05
3.54	0.86	270.83	4.32	1.53	1.77	21.46	1.21	24.85	3.6	0.2	4.2	0.2	931.53	263.14
12.55	5.46	206	16.42	19.22	3.52	23.16	2.96	4.24	42.4	4.8	7.8	0.9	3535.8	281.74
12.51	5.54	246.96	23.776	19.09	3.45	32.89	4.516	5.94	29.7	3.6	5.4	0.6	3429.1	274.11
12.49	5.41	228.19	14.55	19.02	3.52	27.73	3.42	5.13	35.1	3.9	6.5	0.7	3488.8	279.42
12.14	4.78	291.41	35.77	17.98	3.77	37.132	8.66	7.78	24.8	4.7	5.2	1.0	3350.7	276.00
8.76	2.69	355.898	30.73	9.36	3.47	34.33	6	12.75	13.9	2.1	5.2	0.8	2317.1	264.60
6.67	1.65	410.88	31.37	5.42	3.28	43.47	9.34	26.33	6.4	1.1	3.9	0.7	1775.1	266.29
21.60	9.75	428.002	80.294	56.92	5.84	97.6	20.3	10.01	29.8	5.1	3.1	0.5	5750.4	266.22
18.00	8.56	481.33	30.35	39.53	4.62	99.77	7.464	11.66	20.3	1.4	2.4	0.2	4884.7	271.37
14.30	6.81	289.24	21.587	24.95	3.66	46.86	3.795	6.88	27.2	2.0	4.0	0.3	3978.1	278.19
11.60	4.60	213.125	13.45	16.42	3.57	21.058	2.297	4.58	39.9	3.9	8.7	0.9	3118.2	268.81
11.89	4.72	239.45	12.15	17.25	3.65	25.43	2.11	5.38	34.7	2.7	7.3	0.6	3243	272.75
18.73	8.59	509.24	90.725	42.80	4.99	110.3	24.79	12.85	19.8	3.6	2.3	0.4	5171.7	276.12
22.30	10.08	491.95	78.92	60.67	6.02	121.307	22.22	12.03	25.6	4.0	2.5	0.4	6049.7	271.29
21.51	9.50	614.54	95.31	56.45	5.94	152.6	29.62	16.06	18.9	3.1	2.0	0.3	5844.3	271.70
20.57	8.84	611.56	101.65	51.62	5.84	147.24	33.09	16.66	17.9	3.3	2.0	0.4	5666.5	275.47
22.30	10.24	491.95	68.44	60.67	5.92	121.65	17.25	11.88	25.5	3.2	2.5	0.3	6828.6	306.22
24.07	10.69	497.6	75.34	70.68	6.61	131.86	23.14	12.33	27.4	4.1	2.6	0.4	6711.5	278.83
15.06	6.86	284.81	37.07	27.67	4.03	46.36	6.619	6.76	30.5	3.8	4.5	0.556	4269.2	283.48
18.00	7.42	550.468	65.516	39.53	5.33	113.73	20.55	15.33	17.8	2.7	2.4	0.367	5018.5	278.81
15.20	6.99	314.84	27.33	28.19	4.04	54.004	5.462	7.73	26.7	2.5	3.8	0.351	4238	278.82
15.00	6.53	362.07	86.01	27.45	4.21	63.05	18.47	9.66	22.3	5.0	3.4	0.773	4174.1	278.27
17.02	7.32	309.44	64.53	35.34	4.83	54.97	12.49	7.51	32.9	6.1	4.5	0.832	4640.4	272.64

Table 3. Sheet 2 of 2, data for 13-inch spheres.

Vmeas kV	Gap mm	I mean A	SD I A	Input energy mJ	Input energy/ gap mJ/mm	Mean Load Energy µJ	SD load energy µJ	Mean Load Energy/ gap µJ/mm	Effective R spark ohm	3*SD Reff ohm	Rspark/ mm	3*SD Rspark/ mm	Charge nC	Calc cap pF
With 51.15 mohm load														
9.47	3.23	346.08	11.636	10.94	3.39	38.13	3.21	11.82	14.7	1.1	4.5	0.353	2558	270.12
9.55	3.23	337.89	13.406	11.13	3.45	36.49	3.466	11.31	15.6	1.4	4.8	0.419	2610.6	273.36
18.16	8.15	432.61	70.194	40.23	4.93	85.3	16.416	10.46	24.1	3.9	3.0	0.478	4830.2	265.98
17.00	7.62	357.4	52.84	35.26	4.63	67.13	10.666	8.81	26.9	3.7	3.5	0.483	4580.8	269.46
10.38	4.04	250.71	9.529	13.14	3.25	25.39	1.903	6.29	26.5	1.8	6.6	0.457	2807.87	270.51
9.75	3.51	290.15	11.39	11.60	3.31	30.09	2.539	8.58	19.7	1.5	5.6	0.438	2640.5	270.82
7.25	2.20	347.97	7.761	6.41	2.92	33.06	1.97	15.05	9.9	0.6	4.5	0.254	1978.2	272.86
With 204 mohm load														
3.49	0.76	192.26	2.774	1.49	1.95	45.155	1.973	59.26	6.7	0.3	8.8	0.369	901.81	258.40
12.37	5.16	143.99	11.59	18.67	3.62	54.29	7.387	10.53	70.1	8.4	13.6	1.629	3182.9	257.31
17.90	8.08	226.23	44.88	39.09	4.84	140.25	28.99	17.36	56.9	9.7	7.0	1.206	4479.9	250.27
22.10	9.86	260.54	53.84	59.59	6.05	201.72	41.53	20.47	60.3	10.3	6.1	1.044	5548.1	251.05
10.65	3.35	308	29.19	13.84	4.13	131.2	29.19	39.13	21.5	3.9	6.4	1.168	2764.8	259.61
7.28	2.21	255.81	8.215	6.47	2.93	82.09	5.639	37.15	16.1	1.0	7.3	0.467	1928.2	264.86
12.09	4.67	178.46	12	17.83	3.82	62.875	7.558	13.45	57.9	6.2	12.4	1.328	3092.8	255.81
17.00	7.52	325.74	46.19	35.26	4.69	203.7	33.36	27.09	35.3	5.0	4.7	0.661	4324.6	254.39

Appendix: Circuit modeling

In a parallel effort to his experimental work, Prof. C. Durfee and his team at the Colorado School of Mines (CSM) [1] are theoretically modeling the spark formation in great detail. Moreover, at the time of writing they are initiating laser experiments to study spark formation. However, to understand the behavior of the experimental circuit reported here, and how it interacts with the spark, a simpler behavioral model was sought. Of the various published spark models available, for example [6-9], the Braginskii model was found to model our experimental data well and be amenable to inclusion in a simple SPICE circuit model. However, as will be shown, the model has its limitations.

Braginskii Model

The Braginskii model assumes that the spark channel begins as fully-ionized; this is not physically realistic and clearly will not describe the region 1 behavior described in this report. However, it is the region 2 behavior that is primarily of interest to us here because in that region the most energy is transferred to the load. The model then assumes that the specific conductivity of the gas in the spark channel (air here) is constant, only the cross-section of discharge changes with time. The discharge expands as a shock wave in air. Putting a as the radius of discharge, the cross-sectional area ($A = \pi a^2$) which is a function of: initial density of the air (ρ_0 = ~1 kg/m^3 @2286 m LANL-altitude); ξ, a gas constant related to the shock in air; σ the conductivity; and an integral of the current to the 2/3 power. The area becomes

$$A = \pi a^2 = \left[\frac{4\pi}{\rho_0 \xi \sigma}\right]^{1/3} \int_0^t I^{2/3} dt \tag{3}$$

$$R = \frac{len}{A\sigma};\ [\,] \equiv \text{constant}$$

The dynamic spark resistance $R(t)$ is then simply related to the conductivity, length and cross-sectional area at any moment in time (t). For air in SI units: σ = 30 kS/m and ξ = 2.5 are typical values that are derived from published data [6, 10, 11].

One advantage of the model over some others is that it predicts the spark radius, hence we can derive the shock velocity of the gas and "test" the viability of the theory. In practice the predicted radial shock velocities are usually reasonable, but there were notable exceptions i.e., they do not always agree with published data [12], see below.

Model predictions

Circuit predictions, 5-inch sphere, low inductance

The Braginskii model predictions for the 5-inch spheres with an 8.5-mm gap at 21 kV charge, with low inductance, are shown in Figure 17. As can be seen, given the stochastic nature of the experimental results there is fair agreement between the calculated current and the data, both in magnitude and duration.

It is interesting to note the resistance and the channel radius calculated from the model. The channel radius starts from near zero (the circuit model cannot tolerate a true zero) and expands to 64 µm. The spark resistance, derived from the radius, plummets from infinity to a final value of 22 Ω. The measured "effective" spark resistance was 84 Ω ± 29 Ω (3-σ), so there is order-of-magnitude agreement. The calculated energy deposited in the 51.15-mΩ CVR was 9.44 µJ compared to a measured mean energy of 7.35 µJ ± 3.89 µJ (1-σ). Given the scatter in the true data there is fair agreement between calculations and experiment.

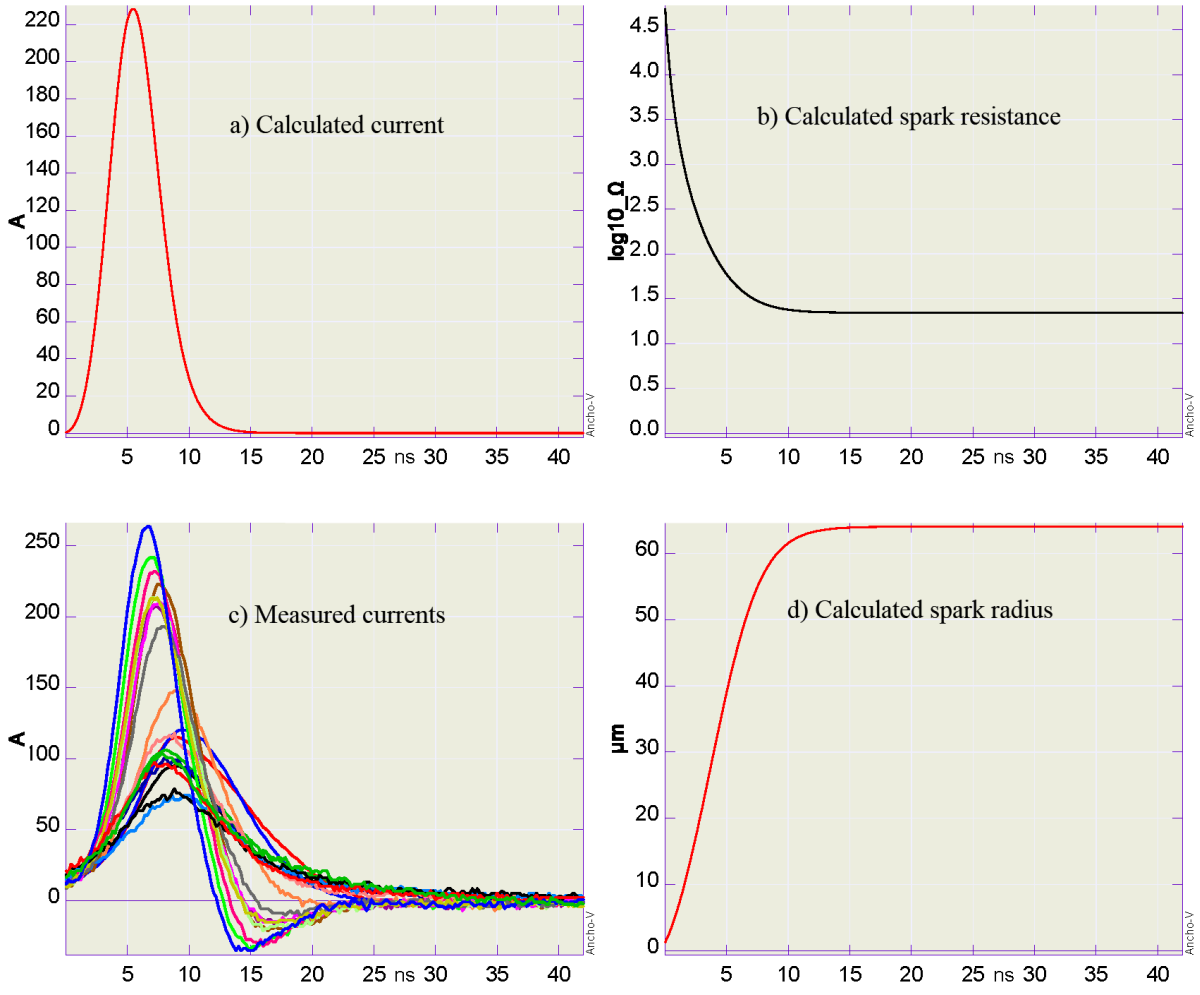

Figure 17. Braginskii model calculations compared to experimental values. 5-inch spheres, 8.5 mm gap, 21 kV charge voltage, low inductance. a) Calculated spark current [A] with a mean of 168 A ± 63 A (1-σ); b) Calculated spark resistance on a scale[log10(Ω)]; c) Measured spark currents for 20 experiments [A]; d) Calculated spark radius [m]. Times 0 to 42 ns.

Radial shock velocity

If the channel radius vs. time data of Figure 17 are differentiated to obtain radial shock velocities, the result produces velocities approaching 9 km/s; this is not physically possible. Comparing this value to known shock velocity data [12] a peak velocity of 3 km/s would be more likely.

Effects of adding inductance to model

The Braginskii model predictions for the 5-inch spheres with an 8.11-mm gap at 21 kV charge, with a 250-nH inductance, are shown in Figure 18. In this case the model over-predicts the current magnitude by perhaps a factor of two.

The calculated spark resistance, derived from the radius, plummets from infinity to a final value of 3.7 Ω. The measured "effective" spark resistance was 200 Ω ± 5 Ω (3-σ), so here the prediction underestimates the resistance by two orders of magnitude. The calculated energy deposited in the 51.15-mΩ CVR was 18.8 μJ compared to a measured mean energy of 3.11 μJ ± 0.08 μJ (1-σ). Here the model over-predicts the energy deposition by almost an order of magnitude.

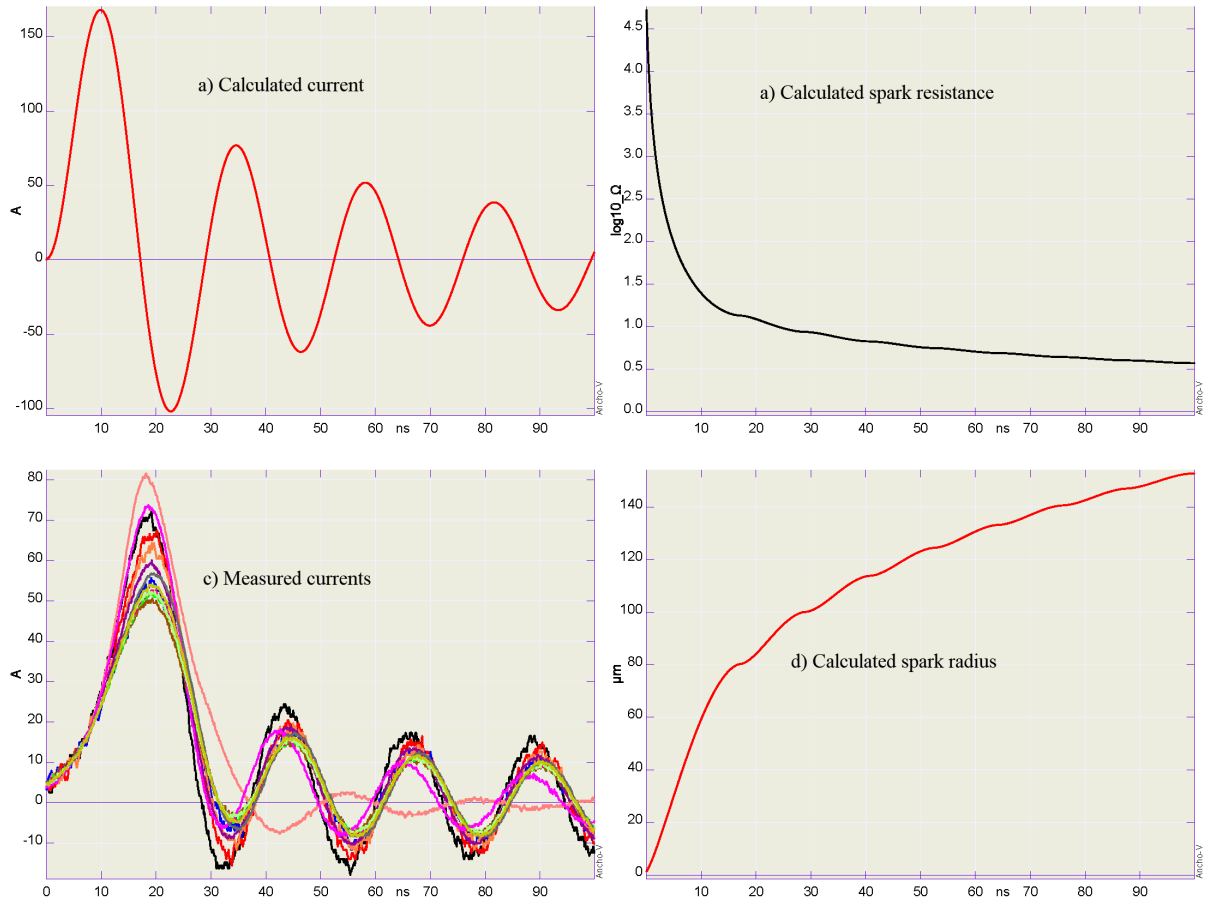

Figure 18. Braginskii model calculations compared to experimental values. 5-inch spheres, 8.1 mm gap, 21 kV charge voltage, 250 nH inductance. a) Calculated spark current [A] with a mean of 62.2 A ± 9.5 A (1-σ); b) Calculated spark resistance on a scale[log10(Ω)]; c) Measured spark currents for 20 experiments [A]; d) Calculated spark radius [μm]. Time scale 0 to 42 ns.

Braginskii model summary

The Braginskii model is a useful tool for predicting current magnitudes and durations with fair accuracy but cannot be considered a realistic physical model of spark behavior because the predicted radial velocities are often too high. However, the values of conductivity σ and the shock constant ξ could be adjusted in Eq.(3) to provide more realistic radii and radial velocities.

Appendix: Prevention of Ground Loops

Errant ringing

When the apparatus was first built, excessive ringing of the current data was observed. To identify the cause of the ground loop(s) a detailed SPICE model was constructed, Figure 19. The cause was eventually identified as a ground loop in the circuit between the power supply and the digitizer that recorded the current data, as described below.

On the left of Figure 19 a 30-kV power supply is represented by the transformer XFMR, diode D and charging capacitor Cpsu. The ground connection to the 120-V AC house power is represented by inductance L1 and capacitance C1. The sphere capacitance Csph is charged via a high voltage resistor chain Rlg = 120 GΩ for the 5-in. spheres. This resistor chain has an estimated stray capacitance of 5 pF and a likely included inductance of 4 µH obtained by conventional estimation techniques [13].

The right of the circuit shows the circuit of the spheres. The sphere capacitance is in series with the inductance of the spheres themselves (estimated to be pH at the most) and the inductance of the spark. [After the following calculations had been completed, and thanks to a conversation with Prof. Durfee from the Colorado School of Mines, this 13-inch sphere inductance was revisited. It is more likely to be 65 nH than the estimated value quoted above.]

This spark inductance varies during the experiment because the radius of the spark increases as the arc channel expands. To model the circuit, this spark inductance has been estimated to be no more than 1 nH [13]. The ammeter (VI) and the voltage source Espk were used to simulate the spark using the Braginskii model, see p. 35. The stray connection resistances to the CVR are estimated to be 10 mΩ (R4, R5, R6 and R7) and the CVR is Rcvr 51.15 mΩ). The output of the CVR is connected to the digitizer by coaxial cables to a 50-Ω termination across the input to the digitizer. The digitizer itself (Xscope) was connected to the house power ground via L2 and C2. (Rbig is a very large and hence negligible

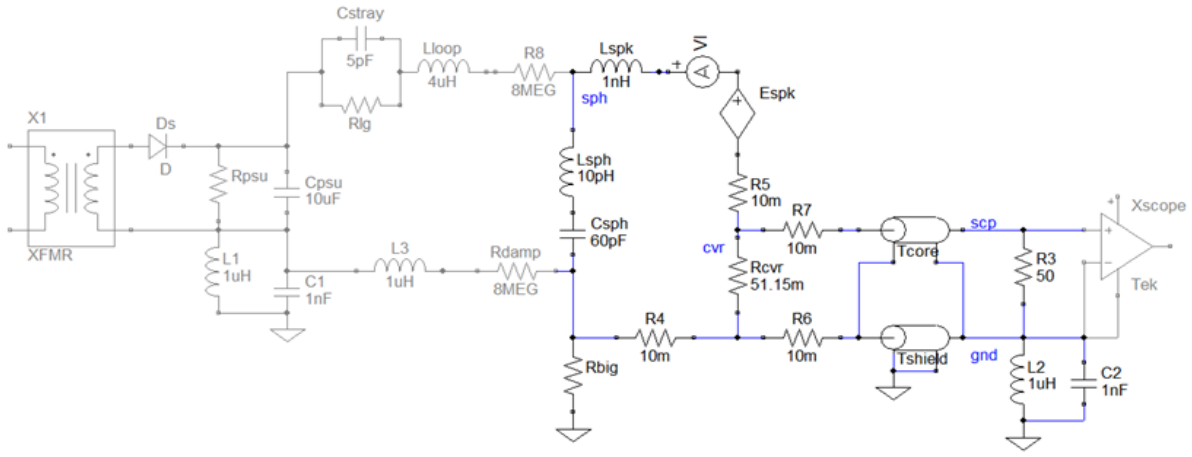

Figure 19. Circuit model of experiment. The greyed components to the left show the ground loop circuit that was essentially eliminated by the isolating resistors, please see the text.

resistance, it is an artifice required to satisfy the DC conditions of the SPICE model without affecting the AC calculations.)

Isolating resistors to suppress ground loop

In the original circuit the two 8-MΩ isolating resistors (R8 and Rdamp) were not included. From the SPICE analysis it was found that (without these resistors) there was a ground loop comprised of L1, L3, R4, R6 and L2. Consequently, there was a direct inductive connection between the ground of the outer sphere and the charging circuit via L3. Whenever the sphere discharged to the CVR significant ringing occurred that corrupted the current data.

By including the isolating resistors the ground loop was broken because in their presence the loop resonance was heavily overdamped. However, the resistance of the isolating resistors was orders of magnitude smaller than the charging resistor and thus had no effect on the charging rate. Now the outer sphere was, in effect, only grounded at the single-point ground of the digitizer via the coaxial cables and good current data were obtained.

References

[1] ‘CSM ESD study, ’ private communications.

[2] ‘AWE Drop-ball ESD experiments,’ private communications.

[3] Tasker, D.: ‘AnchoGraph’, (LANL, 2019, 7.300 edn.), A 32-bit graphics and mathematics package designed for shock wave physics and electrical pulsed power analysis.

[4] ‘Matlab’, (MathWorks, 2019, R2019a edn.), MATLAB is a multi-paradigm numerical computing environment and proprietary programming language developed by MathWorks.

[5] Tasker, D., Bowden, P., Francois, E., Gibson, J., Nakamoto, T., Smith, D., Trujillo, C., and Wilde, Z.: ‘Rogowski Coils for Studies of Detonator Initiation and Other Diagnostics’. Proc. Shock Compression of Condensed Matter, St. Louis, MO2017.

[6] Braginskii, S.: ‘Theory of the development of a spark channel’, SOVIET PHYSICS JETP-USSR, 1958, 7, (6), pp. 1068-1074.

[7] Rompe, R., and Weizel, W.: ‘Über das Toeplersche Funkengesetz’, Zeitschrift für Physik, 1944, 122, (9), pp. 636-639.

[8] Taka, Y., and Fujiwara, O.: ‘Further Validation of Spark-Resistance Formula Applied for Human ESD’, (2009), pp. 393-396.

[9] Toepler, M.: ‘Zur Kenntnis der Gesetze der Gleitfunkenbildung’, Annalen der Physik, 1906, 326, (12), pp. 193-222.

[10] Martin, T., Seamen, J., and Jobe, D.: ‘Energy losses in switches’, Sandia National Labs., Albuquerque, NM (United States). Funding organisation: USDOE, Washington, DC (United States), 1993.

[11] Koppitz, J.: ‘Die radiale und axiale Entwicklung des Leuchtens im Funkenkanal, untersucht mit einer Wischkamera’, ‘Book Die radiale und axiale Entwicklung des Leuchtens im Funkenkanal, untersucht mit einer Wischkamera’ (1967), pp. 1089.

[12] Deal, W.E.: ‘Shock Hugoniot of Air’, J. Appl. Phys., 1957, 28, (7), pp. 782-784.

[13] Grover, F.W.: ‘Inductance Calculations. Working Formulas and Tables’ (Dover Publications, Inc, 2004).